VOID FRACTION IN PARALLEL CHANNEL BOILING WATER REACTORS WITH APPLICATION TO TWO-PHASE TURBULENT MIXING

Ronald Malcolm Reese

VOID FRACTION IN PARALLEL CHANNEL BOILING WATER REACTORS WITH APPLICATION TO TWO-PHASE TURBULENT MIXING

by

RONALD MALCOLM REESE

B.S., U.S. Naval Academy
(1960)

Submitted in Partial Fulfillment of the Requirements
for the Degrees of Naval Engineer and Master of Science
in Mechanical Engineering

at the

MASSACHUSETTS INSTITUTE OF TECHNOLOGY

(June 1970)

ABSTRACT

VOID FRACTION IN PARALLEL CHANNEL BOILING WATER REACTORS WITH APPLICATION TO TWO-PHASE TURBULENT MIXING

RONALD MALCOLM REESE

Submitted to the Department of Naval Architecture and Marine Engineering on June 4, 1970, in partial fulfillment of the requirements for the degrees of Naval Engineer and Master of Science in Mechanical Engineering.

An experiment using air-water mixtures to model steam-water flow in a reactor was devised to determine the turbulent mixing mass flow rates between two subchannels over a wide range of flow conditions and therefrom predict turbulent mixing occurring in the reactor. An experimental apparatus was constructed for this experiment.

Void fraction was chosen as a plausible correlating parameter for turbulent mixing and was measured together with axial pressure gradient for two subchannel geometries of interest.

The subchannel geometries investigated were those found in a typical BWR fuel bundle. The flow regime in the subchannels was detected by means of an electric conductivity probe and visual observations. Data obtained are compared with various correlations.

Predictions of void fraction and pressure gradient with the Lockhart-Martinelli correlation agreed closely with the data. Comparisons were also made with Griffith's slug flow model, and with the Cravarolo-Hassid and Marchaterre-Hoglund void fraction correlations.

Thesis Supervisor: Borivoje B. Mikic
Title: Associate Professor of Mechanical Engineering

Acknowledgements

The research work performed in this thesis was sponsored by the General Electric Company, Atomic Power Equipment Department, San Jose, California.

The author wishes to thank Professor George Yadigaroglu for his interest and assistance in this work, Mr. Fred Johnson for his technical assistance in the construction of the apparatus and Miss Sandra Vivolo for the typing of the manuscript.

The assistance of my wife, Ann, in the preparation of the manuscript, is deeply appreciated.

Table of Contents

LIST OF SYMBOLS

A = subchannel cross sectional area (FT^2)

c = rod gap width (FT)

C_o = two-phase velocity and concentration distribution parameter (dimensionless)

$\left(\frac{dp}{dl}\right)_{FR\ \ell}$ = frictional pressure gradient if the liquid phase flowing alone were allowed to fill the entire channel (LB_f/FT^2-FT)

$\left(\frac{dp}{dl}\right)_{FR\ TP}$ = frictional two-phase pressure gradient (LB_f/FT^2-FT)

$\left(\frac{dp}{dl}\right)_{ELEV\ TP}$ = two-phase elevation pressure gradient (LB_f/FT^2-FT)

D_e = hydraulic diameter (4A/P) (FT)

f = single phase liquid friction factor (dimensionless)

f_D, f_T = diversion cross flow/turbulent mixing momentum exchange multiplier

F = friction force per unit length at the subchannel wall (LB_f/FT)

g = acceleration due to gravity (FT/HR^2)

g_c = conversion factor ($LB_m FT/LB_f HR^2$)

G = mass velocity or mass flux ($LB_m/HR\ FT^2$)

G_i, G_j = mass velocity in subchannel i, j in the axial direction ($LB_m/HR\ FT^2$)

G_{ij}', G_{ji}' = turbulent mixing mass velocity from subchannel i to j and vice versa ($LB_m/HR\ FT^2$)

G_{mixing} = net turbulent mixing mass velocity ($LB_m/HR\ FT^2$)

h = enthalpy (BTU/LB_m)

j = local volumetric flux density ($FT^3/HR\ FT^2$) = $V_g\alpha + V_f(1-\alpha)$

j_g = local gas volumetric flux density ($FT^3/HR\ FT^2$)

ℓ = mixing length (FT)

L = communication (window) length (FT)

m_i, m_j = inlet mass flow rate in subchannel i, j or exit mass flow rate under isolated conditions (LB_m/HR)

m_i^*, m_j^* = exit mass flow rate from subchannel i, j when subchannels are communicating

p = pressure (LB_f/FT^2)

Q = volume flow rate (FT^3/HR)

q = heat flow per unit length of subchannel (BTU/HR FT)

S = slip ratio (V_g/V_f, local; $\bar{V}_g/\bar{V}_f$, average) (dimensionless)

u = axial velocity (FT/HR)

$u_{ij,g}$; $u_{ji,g}$ = diversion cross flow velocity from subchannel i to j and vice versa for gas and liquid

$u_{ij,f}$; $u_{ji,f}$ respectively (FT/HR)

$|\overline{u_{ij,g}}|$ = representative measure of the fluctuating turbulent mixing gas velocity from subchannel i to j (e.g., RMS value or average of absolute value) (FT/HR)

$|\overline{u_{ij,f}}|$ = representative measure of the fluctuating turbulent mixing liquid velocity from subchannel i to j (e.g., RMS value or average of absolute value) (FT/HR)

v' = mean flowing two-phase specific volume (FT^3/LB_m), Appendix A

V_f = local liquid velocity (FT/HR)

V_g = local gas velocity (FT/HR)

$\bar{V}_g$ = weighted mean gas velocity (FT/HR) = $\frac{Q_g}{A_g} = \frac{Q_g}{\alpha A}$

$\bar{V}_f$ = weighted mean liquid velocity (FT/HR) = $\frac{Q_f}{A_f} = \frac{Q_f}{A(1-\alpha)}$

V_{gj} = local gas drift velocity ($V_g - j$) (FT/HR)

$\bar{V}_{gj}$ = weighted mean gas drift velocity (FT/HR)

w_{ij}, w_{ji} = diversion cross flow mass flow rate per unit length from subchannel i to j and vice versa (LB_m/HR FT)

w_{ij}', w_{ji}' = turbulent mixing mass flow rate per unit length from subchannel i to j and vice versa (LB_m/HR FT)

w'_{net} = net turbulent mixing mass flow rate per unit length (LB_m/HR FT)

X = flowing quality, (m_g/m_g+m_f) (dimensionless)

α = void or gas volumetric fraction, (A_g/A) (dimensionless)

β = average mass velocity multiplier for turbulent mixing in the COBRA Code (Mixing Stanton Number) (dimensionless)

ρ = average density (LB_m/FT^3) $(\rho_f(1-\alpha) + \rho_g\alpha)$

ϕ_ℓ^2, ϕ_g^2 = liquid and gas two-phase frictional pressure multipliers (dimensionless)

$< >$ = denote cross sectional averages, $\langle f \rangle = \frac{1}{A}\int_A f dA$

Subscripts

eq = refers to equilibrium conditions

f = refers to liquid phase

g = refers to gas phase

i = refers to ith subchannel

j = refers to jth subchannel

List of Figures

CHAPTER I

Introduction

The core of modern boiling water reactors is composed of a large number of subassemblies or fuel bundles. Each subassembly contains a matrix of vertical, cylindrical, parallel fuel rods. The fuel bundles are generally enclosed in a surrounding unheated wall. Figure 1 shows such a typical 16-rod bundle arranged on a square array. The main coolant flow is vertical, parallel to the axis of the subassembly. However, secondary radial flows between adjacent rods and between the outer rods and the wall also take place.

The assumption is generally made that the phenomenon known as critical heat flux (CHF), burnout, or departure from nucleate boiling (DNB) depends only upon the local conditions. The prediction, then, of the location and the magnitude of the CHF requires a complete and detailed knowledge of the main and secondary flow patterns.

Accurate estimation of the magnitude of the secondary flows, known as mixing, has been the major problem in the prediction of the critical heat flux condition. Considerable progress has been made in the area of mixing flows in single phase flow. The mechanisms of two-phase mixing, however, are still not well understood.

It has been convenient to subdivide the main flow through the rod bundle or subassembly into flows between four adjacent rods or between a rod or rods and the subassembly wall. Such

artificially defined flow ducts are generally referred to as rod channels or subchannels.

The standard approach to a thermal-hydraulic analysis of a rod bundle utilizes these subchannels. A typical subchannel breakdown of a rod bundle is illustrated in Figure 1. Mean properties are assigned to each subchannel. Thus a mean axial velocity, enthalpy, void (or volumetric) fraction is assumed to exist over the entire cross section of a subchannel. This lumped parameter approach, although far from being strictly correct, serves as a first approximation to the actual velocity, enthalpy and concentration profiles existing in a given subchannel.

Mixing between parallel, ventilated (communicating) rod channels has been conveniently defined by Todreas and Rogers (2) as follows:

Natural mixing

a) Turbulent interchange

b) Diversion cross flow

Forced mixing

a) Flow scattering

b) Flow sweeping

Turbulent interchange is caused by the fluctuating velocities and pressures present in turbulent flow and has been broadly defined as a no net mass transfer phenomenon, in accordance with Prandtl's mixing length theory. Such a definition has application to single phase flow but requires revision for two-phase flow.

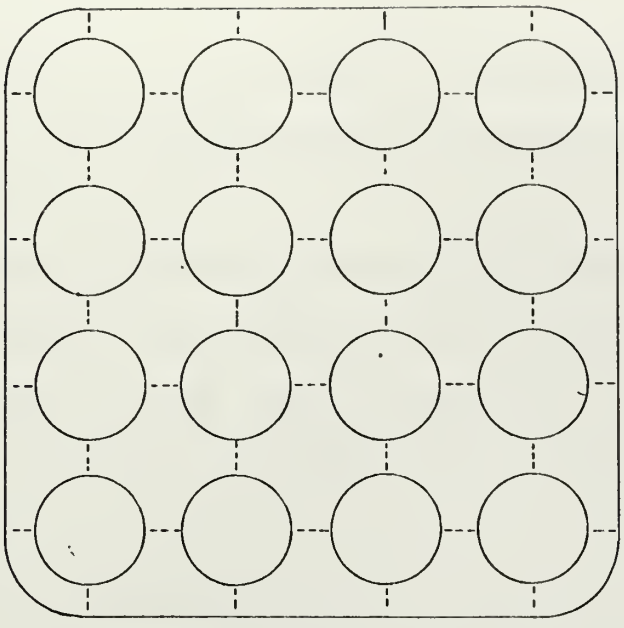

16 ROD BUNDLE

A

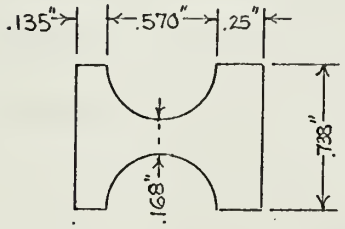

B

C

SUBCHANNEL GEOMETRIES OF INTEREST

ROD BUNDLE SHOWING SUBCHANNELS
FIGURE 1

Diversion cross flow is the net secondary flow resulting from a static pressure difference between parallel channels at a given level within the rod bundle. In general, it will be represented by a net mass transfer for single and two-phase flow conditions.

Forced mixing, by flow scattering and flow sweeping, is artificially induced. Rod spacers, for example, may produce a random diversion of flow (flow scattering). Devices such as helical rod wraps produce a preferential diversion of flow (flow sweeping).

In the realm of natural mixing it has been assumed that the mechanisms of turbulent interchange and diversion cross flow are independent or at least may be analyzed as such as a first approximation. As noted by Todreas and Rogers (2), where large diversion cross flows exist, this probably is an erroneous assumption, but nevertheless, it has been a reasonable method of attacking the mixing problem.

The magnitude of the mixing flows has been investigated by Rowe and Angle (1), (8) and by Lahey, Shiralkar and Radcliffe (3) for the diabatic case. Rowe and Angle investigated turbulent interchange by using radioactive tracers. This method could not, however, give the net mixing vapor and liquid mass flow rates between two channels. It has been shown (e.g. (3)) that the vapor has an affinity to migrate to the less restricted regions of the central channels away from the unheated bundle walls.

It would appear, then, that two phase natural mixing in the absence of a radial pressure gradient may be caused by at least two phenomena: 1) turbulent interchange, as in single-phase flow, and 2) a bubble drift to less restricted flow areas.

In spite of this information, in this thesis natural mixing flow in the absence of a radial pressure gradient will continue to be referred to as turbulent mixing. This is in concurrence with most literature.

The mechanism of diversion cross flow seems to be fairly well understood, and the magnitudes of these flows can be estimated by simply modeling the rod gap as an orifice subjected to a pressure difference.

The mechanisms of turbulent mixing flows, on the other hand, are not at all well understood, and past estimates have often been based on crude and somewhat arbitrary models. A typical method has estimated the turbulent mixing mass velocity, G_{mixing}, as equal to some constant, β, multiplied by the average mass velocity of adjacent subchannels.

$$G_{mixing} = \frac{w'_{ij}}{c} = \beta \frac{(G_i + G_j)}{2}$$

where w'_{ij} is the mixing mass flow rate per unit length and c is the rod gap spacing.

With this background, it can be seen that a more accurate determination of the magnitude and mechanisms of turbulent mixing flows is required.

It was decided, then, to construct an apparatus which could determine the magnitude of the turbulent mixing flows over a wide range of flow conditions. This apparatus, hopefully, could also give some insight into the mechanisms of two-phase turbulent mixing. Such an apparatus would have to exclude the possibility of diversion cross flow mixing and thus measure only the turbulent mixing component. This could be accomplished if pressure level and pressure drop could be equated at corresponding points in two adjacent subchannels, thus removing the driving force for diversion cross flow. As a first approximation, such an experiment could be conducted under adiabatic conditions with air and water, modeling the steam-water flow of the reactor. Particular subchannels of interest are shown in Figure 1. Subchannel geometry (b) was selected initially and is that geometry investigated in this thesis.

It was furthermore postulated that void fraction might serve well as a correlating parameter for turbulent mixing. An indication of the influence of void fraction on mixing is the experimental evidence obtained by Rowe and Angle (8) and Lahey et al. (3), who showed mixing to be a function of quality, peaking somewhere in the slug flow regime.

The purpose of this research work was the experimental determination of void fraction over a wide range of air and water mass flow rates for a typical rod bundle subchannel geometry. Simultaneously, pressure level and pressure drop were recorded and flow regimes were identified. Thus a

complete picture of the flow conditions was determined for a wide range of operating conditions. The data obtained have been compared with various correlations, and similarities and differences are discussed.

CHAPTER II

Theory

It is generally accepted that steam-water mixtures may, under certain conditions, be accurately modeled by air-water mixtures. In the present case this greatly simplifies the equipment necessary for the study of two-phase turbulent interchange.

As previously stated, turbulent interchange is defined as the mass transfer occurring in the absence of a static average pressure difference between adjacent subchannels at a given axial position. Hence, any experiment designed to determine this mixing flow would necessarily require equating pressure level and pressure drop at corresponding points in the subchannels. By establishing flows meeting these conditions with unequal void fractions in adjacent subchannels, one could observe the net mixing mass flow rates of air and water.

The mixing flow rates could be obtained if some means were provided for isolating the two subchannels upstream and downstream of a communication length, by simply measuring the flow rates of air and water in the two subchannels. This method is probably most accurate when the flows in the adjacent subchannels have distinctly different qualities.

The net mixing mass flow rates could also be determined from the difference in the inlet and exit air and water mass flow rates of each channel, with the channels continuously in communication. However, the maintenance of unequal void

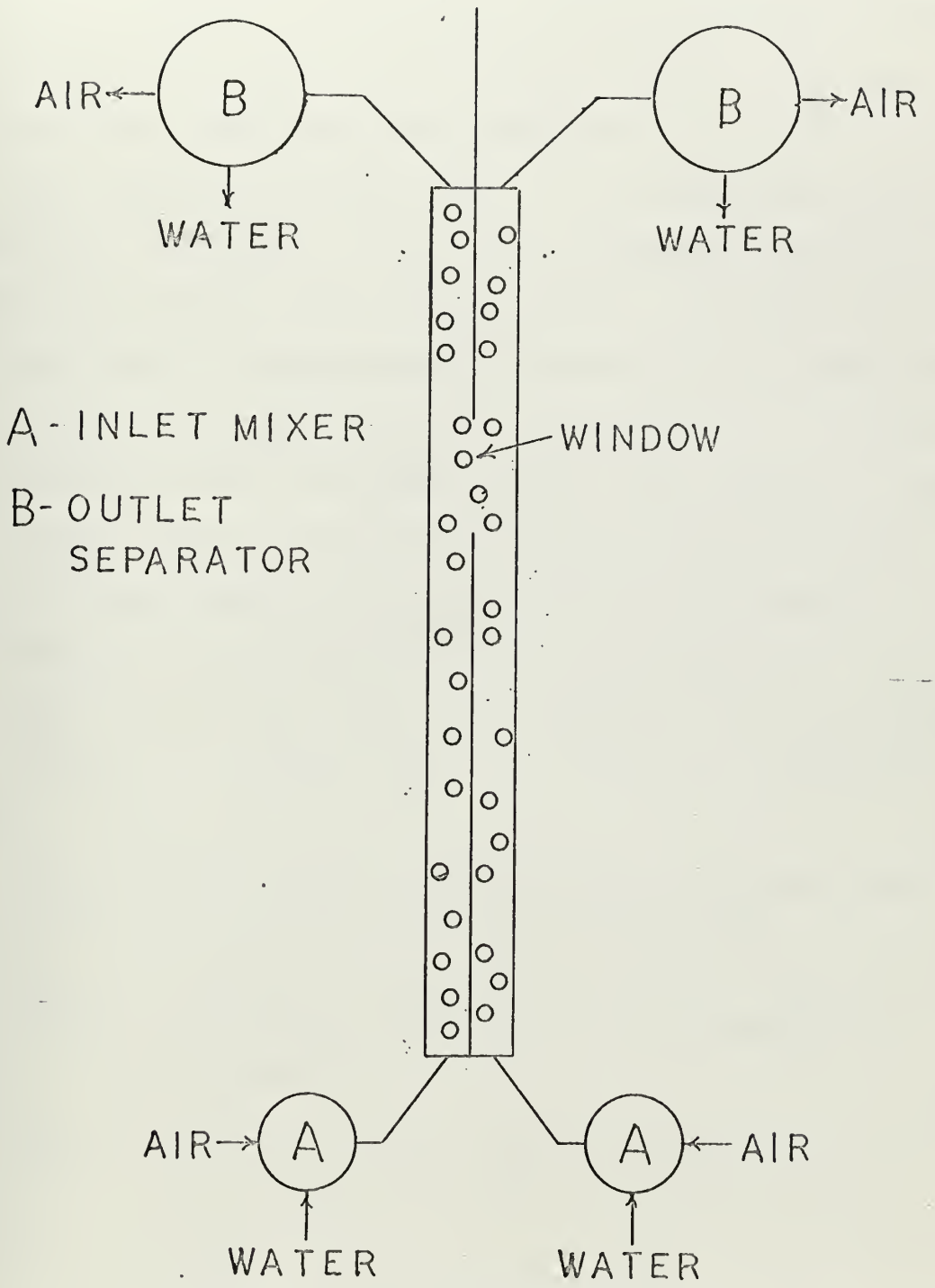

BASIC MIXING APPARATUS

FIGURE 2

fractions and yet equal pressure and pressure gradients under these conditions is difficult if not impossible. Furthermore, in the first method, conditions of fully developed flow can be attained prior to allowing mixing to occur. This was thought to be a more realistic approach.

The operating procedure then is to completely isolate the subchannels, establish flows in each subchannel satisfying the conditions of equal pressure and pressure gradient, and measure the flow rates. Subsequently, a portion of the common boundary, the rod gap, is opened (that is, the subchannels are allowed to communicate over a variable length, the "window"). With the "window" open, the exit flow rates are measured again and the net mixing flows of air and water are calculated.

This net liquid mixing flow is then given by:

$$w'_{net,f} \cdot L = (w'_{ji,f} - w'_{ij,f}) \cdot L = m_{i,f}^{*} - m_{i,f} = -(m_{j,f}^{*} - m_{j,f})$$

where

$w'_{net,f}$ = net liquid turbulent mixing mass flow rate per unit length of channel (LB_m/HR FT)

$w'_{ij,f}$ = turbulent mixing liquid mass flow rate per unit length from subchannel i to subchannel j (LB_m/HR FT)

$w'_{ji,f}$ = turbulent mixing liquid mass flow rate per unit length from subchannel j to subchannel i (LB_m/HR FT)

L = length of communication (FT)

$m_{i,f}; m_{j,f}$ = exit mass flow rates of liquid from the ith and jth subchannels under isolated conditions (LB_m/HR)

$m^*_{i,f}$; $m^*_{j,f}$ = same as $m_{i,f}$; $m_{j,f}$, except that subchannels are allowed to communicate

A similar expression can be written for the net gas turbulent mixing mass flow rate.

$$w'_{net,g} \cdot L = (w'_{ji,g} - w'_{ij,g}) \cdot L = m^*_{i,g} - m_{i,g} = -(m^*_{j,g} - m_{j,g})$$

The net total mixing mass flow rate is $w'_{net} = w'_{net,f} + w'_{net,g}$.

The window length, L, will necessarily be chosen through experimentation. Hopefully, by measuring the mixing mass flow rates with decreasing lengths of communication, differential values can be obtained at the limit by extrapolation to a zero window opening.

Subchannel geometry (b) Figure 1, selected for initial investigation, is representative of a typical wall subchannel on the left side of the rod gap. The right side of the rod gap models approximately a central rod bundle subchannel, such as that existing between four rods.

A recognized artificiality in this experiment is the effect of the imposition of a wall at the rod gap to isolate the channels. Since the width of the rod gap (.168") is small in comparison to the total perimeter (2.071" and 2.301" for the left and right channels, respectively), it may be argued that the effect on the overall flow conditions is small. However, the abrupt termination of this wall at the beginning of the communication window in the mixing apparatus will have some effect upon mixing. The eddies produced by the vorticity in the boundary layer undoubtedly will cause some additional

mixing. It is argued, however, that with sufficiently long window opening, the true turbulent mixing flows to be measured will dominate the artificially induced effects due to boundary layer vorticity.

A further effect of the presence of an isolating wall between the subchannels is the deviation of the void fraction distribution from that which would exist if no wall were present at the rod gap. It is expected, also because of the narrow rod gap, that this effect will be small. Nevertheless, if the two-phase mixing length is found to be on the order of magnitude of the rod gap width, (i.e., if the average subchannel properties are not representative of the local conditions where mixing occurs) concentration profiles in the communicating channels will probably have to be investigated.

The net mixing mass flow rate per unit length for gas and liquid combined can be postulated to be a function of the average void fraction, α, as follows:

$$w'_{net} = w'_{ji} - w'_{ij} \cong c[(\alpha_i - \alpha_j)\rho_f|\overline{u_{ij,f}}| + (\alpha_j - \alpha_i)\rho_g|\overline{u_{ij,g}}|]$$

In this formulation c is the rod gap spacing and $|\overline{u_{ij,f}}|$ and $|\overline{u_{ij,g}}|$ are representative measures of the turbulent fluctuating velocities of the liquid and gas respectively, e.g., RMS values or averages of the absolute values.

The conservation equations and the turbulent mixing equation given above are developed in detail in Appendix A.

Since the net liquid and gas mixing flows are expected to be some function of the void fractions in the communicating channels, a detailed knowledge of void fraction is required over a wide range of water and air mass flow rates. In order to match pressure level and pressure drop at unequal void fractions, a knowledge of pressure drop as a function of void fraction would also be desirable. Lockhart and Martinelli (5) have shown the void fraction and pressure gradient to be functions of gas and liquid density, and hence, functions of pressure level. For this reason, the pressure level at the location of the communicating window is also of interest.

Void fraction data for air-water and other two-phase mixtures in horizontal round tubes has been correlated by Lockhart and Martinelli (5) using a parameter, X, which is a function of flowing quality, density and viscosity of the two phases. This same parameter, X, is also used to correlate the two-phase frictional pressure drop, $dp/dl)_{FR\ TP}$ to the single-phase gas or liquid pressure drop through the pressure drop multiplier, ϕ^2, where

$$\frac{dp}{dl})_{FR\ TP} = \phi_{\ell}^2 \frac{dp}{dl})_{FR\ \ell} = \phi_g^2 \frac{dp}{dl})_{FR\ g}$$

The subscripts T.P., ℓ, and g refer to two-phase, liquid only, or gas only (respectively) filling the entire tube. Thus, for given liquid and gas mass flow rates, it is possible to predict the void fraction, α, and the two-phase frictional pressure drop.

The elevation pressure drop is given by

$$\left(\frac{dp}{dl}\right)_{ELEV\ TP} = \rho g/g_c = [\rho_f(1-\alpha) + \rho_g\alpha]\ g/g_c$$

Hence, using the Lockhart-Martinelli correlation, the total pressure drop may be predicted.

$$\left(\frac{dp}{dl}\right)_{TOTAL\ TP} = \left(\frac{dp}{dl}\right)_{FR\ TP} + \left(\frac{dp}{dl}\right)_{ELEV\ TP}$$

Void fraction correlations of other authors (12), (13) are also used in this work.

Another parameter of interest in two-phase flow is the ratio of average gas velocity to average liquid velocity, known as the velocity ratio or slip ratio.

$$S = \frac{\bar{v}_g}{\bar{v}_\ell}$$

As noted by Zuber and Findlay (9), in a flow channel, local slip ratios exist as well as a local concentration (void fraction) profile. Knowledge of local void fraction may be helpful in the determination of a mixing length for turbulent mixing. Zuber and Findlay have defined a parameter, C_o, which is a measure of the peaking of the concentration and velocity profiles. Average void fraction data for a wide range of flow rates provides sufficient information for estimation of C_o.

For round tubes, Zuber and Findlay assumed velocity and concentration distributions as follows:

$$\frac{j}{j_c} = 1 - \left(\frac{r}{R}\right)^m$$

$$\frac{\alpha-\alpha_w}{\alpha_c-\alpha_w} = 1 - \left(\frac{r}{R}\right)^n$$

where j is the local volumetric flux density of the mixture ($FT^3/HR\ FT^2$) and the subscripts c and w refer to conditions at the centerline and the wall respectively.

The distribution parameter C_o is defined as

$$C_o = \frac{1/A \int_A \alpha j dA}{[1/A \int_A \alpha dA] \cdot [1/A \int_A j dA]} = \frac{\langle \alpha j \rangle}{\langle \alpha \rangle \langle j \rangle} = 1 + \frac{2}{m+n+2}\left(1 - \frac{\alpha_w}{\langle \alpha \rangle}\right)$$

where the brackets, < >, denote cross sectional average values.

It is evident that for adiabatic flow ($\alpha_w = 0$)

$$C_o = \frac{m + n + 4}{m + n + 2}$$

For triangular concentration and velocity profiles ($m = n = 1$), C_o reaches a maximum of 1.5. With values of m and n between 2 and 3 parabolic profiles are produced, similar to the velocity profiles for single-phase laminar flow. Higher values of m and n (~7) produce profiles similar to turbulent velocity profiles. As a flatter profile of concentration and velocity is reached, C_o approaches a value of unity.

Zuber and Findlay have also shown that the weighted mean gas velocity $\bar{V}_g$ may be expressed in terms of C_o and a weighted mean gas drift velocity $\bar{V}_{gj}$

$$\bar{V}_g = \frac{\langle j_g \rangle}{\langle \alpha \rangle} = \frac{\langle \alpha V_g \rangle}{\langle \alpha \rangle} = C_o \langle j \rangle + \bar{V}_{gj}$$

where $V_{gj} = V_g - j$ is the local drift velocity of the gas,

$$\langle j \rangle = \frac{Q_g + Q_f}{A}$$

$$\langle j_g \rangle = Q_g / A$$

and

$$\bar{V}_{gj} = \frac{\langle \alpha V_{gj} \rangle}{\langle \alpha \rangle}$$

Hence, C_o can be determined from the slope of a $\bar{V}_g$ versus $\langle j \rangle$ plot, and the weighted mean drift velocity from the intercept with the ordinate axis. A typical plot in the $\bar{V}_g$ - $\langle j \rangle$ plane is given below.

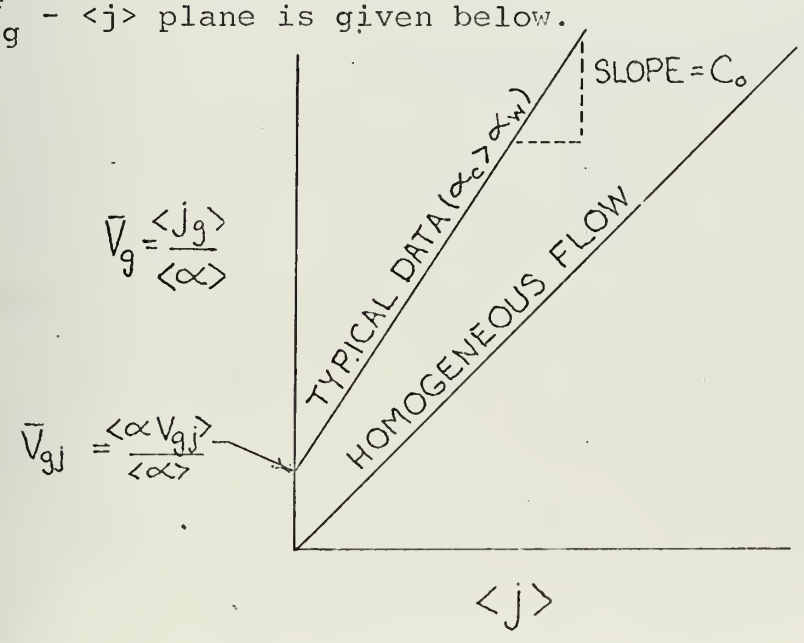

Hence it can be seen that plotting $\bar{V}_g$ versus <j> over a wide range of flow conditions will yield, at least for round tubes, some information on the void and velocity profiles in the flow duct. Additional information on concentration profiles could be provided by a traversing void fraction probe, if necessary.

The role of mixing length, ℓ, in two phase turbulent mixing is of importance if one considers the net mixing mass flow rate, w'_{net}, as a function of a void fraction eddy diffusivity, ε_α, and a concentration gradient, $\frac{d\alpha}{dy}$.

$$G_{mixing} = \frac{w'_{net}}{c} = \rho_j|\overline{u_{ij}}| - \rho_i|\overline{u_{ij}}|$$

$$= [\rho_f(1-\alpha_j)+\rho_g\alpha_j]\ \ell\frac{du}{dy}$$

$$- [\rho_f(1-\alpha_i)+\rho_g\alpha_i]\ \ell\frac{du}{dy}$$

$$= (\rho_f-\rho_g)(\alpha_i-\alpha_j)\ \ell\frac{du}{dy}$$

$$= (\rho_f-\rho_g)\frac{(\alpha_i-\alpha_j)}{\ell}\ [\ell^2\ \frac{du}{dy}]$$

$$\cong (\rho_f-\rho_g)\ \varepsilon_\alpha\frac{d\alpha}{dy}$$

where

$$\varepsilon_\alpha \equiv \ell^2\ \frac{du}{dy}$$

and

$|\overline{u_{ij}}|$ = appropriate measure of the turbulent mean fluctuating velocities of liquid and gas, here assumed to be equal (FT/HR)

G_{mixing} = net mixing mass velocity ($LB_m/HR\ FT^2$)

y = direction perpendicular to the main flow between adjacent rods

u = local axial velocity

The subchannel densities (ρ_i, ρ_j) here refer to average representative values in the two subchannels.

With knowledge of the mixing flow rates and void fraction profiles it may be possible to determine at least the order of magnitude of ℓ, the two-phase mixing length. Although several investigators have proposed that G_{mixing} is independent of rod gap spacing, c, and dependent rather on hydraulic diameter, other investigators have proposed the opposite. Lahey and Schraub (11) discuss this matter at length. The order of magnitude of the mixing length, ℓ, may shed some light on this controversy.

While the above formulation seems intuitively correct, there are indications that it is probably true only under certain conditions. One such condition might be the case of two identical subchannels in communication. In this case when the void fractions are equal, $(\frac{d\alpha}{dy} = 0)$, one would expect zero net mixing.

A broader view of this problem, however, suggests viewing the two subchannels in communication as a single channel progressing toward a condition of equilibrium concentration and velocity distributions.

When one considers a subchannel geometry such as geometry (a) in Figure 1, the equilibrium void fraction distribution probably would not be one with $\frac{d\alpha}{dy} = 0$. This supposition is supported by work discussed by Lahey and Schraub which shows that there is a distinct variation in equilibrium void fraction from the corner subchannel (geometry (a), Figure 1) and the centermost subchannels of the rod bundle. Such evidence supports the concept of a bubble drift mixing effect, previously mentioned in Chapter I.

If $\rho_{i,eq}$ and $\rho_{j,eq}$ refer to average representative densities in the two subchannels under equilibrium conditions, then, using the same notation as before, one can show

$$G_{mixing} = (\rho_j - \rho_{j,eq})|\overline{u_{ij}}| - (\rho_i - \rho_{i,eq})|\overline{u_{ij}}|$$

$$\cong (\rho_f - \rho_g)\ \varepsilon_\alpha \left(\frac{d\alpha_{eq}}{dy} - \frac{d\alpha}{dy}\right)$$

Despite the fact that the influence of void fraction on turbulent mixing is not well understood, it would seem that a first step in any such investigation is the determination of average void fraction over a wide range of flow conditions for a given geometry.

There are several experimental methods for measuring average void fraction. The simplest method is the use of quick closing isolation valves. If the valves can be shut simultaneously and sufficiently fast to trap a representative sample of the two-phase mixture, the trapped liquid can be metered to give accurately the average void fraction. The

application of this method to a non-circular duct necessitated the maintenance of the flow duct geometry throughout the valves in order to avoid perturbation of the flow.

CHAPTER III

Description of Apparatus

General

The apparatus utilized to determine the required data was a basic air-water system with filters, pressure regulators and surge tanks for air and water, mixing devices, test sections, air-water separators and flow measuring devices. Other instrumentation provided were air and water temperature and pressure measurement, pressure drop measurement, and electric flow regime detection. The void fraction determination was accomplished by quick closing valves and read directly through a transparent test section of lucite. Figure 3 is a schematic representation of the overall experimental apparatus. Letters in parentheses throughout this section represent the various portions of the apparatus as indicated in Figure 3.

Figure 4 is a photograph showing the major portion of the apparatus. On a support framework consisting of Dexion strengthened by plywood was mounted the three foot entrance section (Q) and the five foot interchangeable test sections (S), simulating reactor subchannels. The filters (B,F), pressure regulators (C,G) and surge tanks (D,H) were located on the lower level with the mixing devices (N) located directly under the lucite entrance section.

At the exit of the vertical test sections (V) and on the upper level of the laboratory, two identical air-water separators were mounted, one separator for each subchannel.

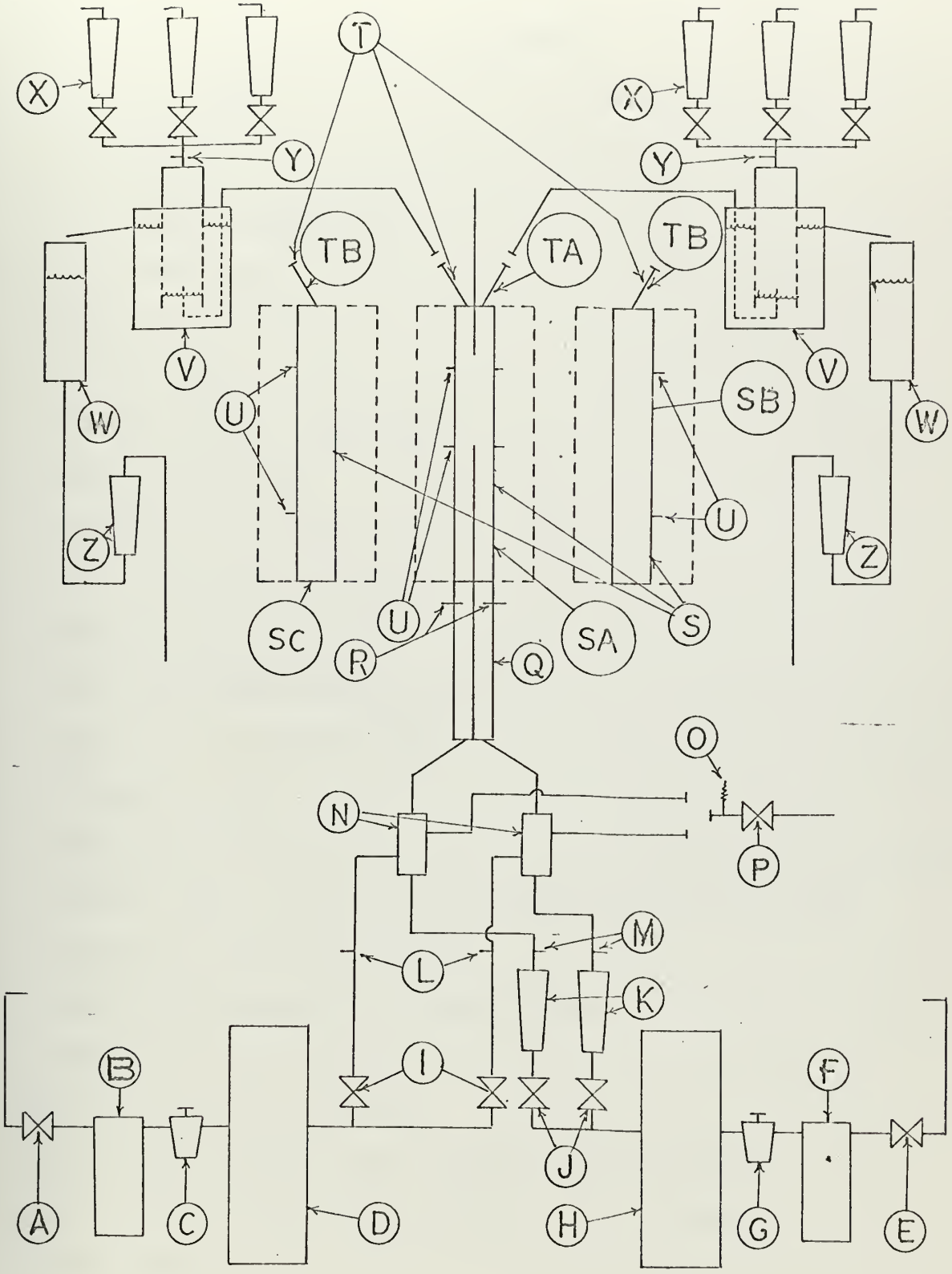

OVERALL APPARATUS - SCHEMATIC

FIGURE 3 KEY ON NEXT PAGE

Key to Figure 3

A - Air root value

B - Air Filter

C - Air pressure regulator

D - Air surge tank

E - Water root value

F - Water filter

G - Water pressure regulator

H - Water surge tank

I - Air throttle valves

J - Water throttle valves

K - Water inlet rotameters

L - Air inlet thermocouples

M - Water inlet thermocouples

N - Mixing devices

O - Bypass relief valve (in use for void fraction testing only)

P - Bypass valve (in use for void fraction testing only)

Q - Three foot entrance section

R - Electric conductivity (flow) probes

S - Five foot test sections

    SA - Mixing test section

    SB - Void fraction test section--right channel

    SC - Void fraction test section--left channel

T - Exit blocks

    TA - Mixing section exit block

    TB - Void fraction section exit block

U - Pressure taps

V - Air-water separators

W - Water spill receiving tank

X - Outlet air flow rotameters

Y - Outlet air thermocouples

Z - Outlet water rotameters

Photograph of Overall Apparatus

Figure 4

Air flow measurement was accomplished by use of rotameters (X) at the exit of the air from the separators. The air flow meters exhausted to the atmosphere. Because of the wide range of air flow to be measured, a bank of flowmeters with changeable floats was provided to meet the anticipated flows.

The Martinelli-Nelson correlation for void fraction versus quality was used to determine the steam-water void fraction corresponding to the maximum local quality existing in a boiling water reactor at 1000 psig. Using this same void fraction for air-water, the Lockhart-Martinelli (5) and Wallis (4) correlations were used to predict anticipated air flow rates for a maximum water mass velocity of 1×10^6 LBm/HRFT^2. Because of the large number of flowmeters required, air flow measurement was initially installed only at the exit of the separators. Thermocouples (Y) were installed prior to the air flow rotameters.

Water flow measurement, also by rotameters, was provided both prior to the mixing devices (K) and at the exit of the separators (Z).

From the beginning it was recognized that the inaccuracy of the rotameters (±.5% repeatability) might present problems in determination of the small mixing flows but would be adequate for void fraction determination. The advantages of a continuous rather than an intermittent device and the high flow rates anticipated for the higher void fractions led to the decision to utilize flow meters rather than an intermittently

operated receiving tank for flow measuring. Data using the mixing test section indicates however, that an intermittent flow measuring device will indeed be required, primarily because of fluctuations in the air flow at very low and very high flow rates.

Separators

The separators themselves used an inverted burette principle. The air-water mixture emanating from the test sections was introduced into an inverted "can" in a larger spill tank (see Figure 5). The level in the outer spill tank was kept constant by the spillway, while the level in the inner can varied with air flow rate. The air-water mixture was separated by gravity and by inertial forces by use of baffles in the top portion of the inner "can". The water spilled into a spill collection tank from which it was routed to an exit water flow meter. Slight variations in the water level in the inner can caused by the separation process were thought to be the cause of the air flow fluctuations.

Mixing Device and Air and Water Supplies

The mixing device (N) is shown in detail in Figure 6. The air was introduced radially into the water stream by a small pipe closed at the end and drilled with small holes along its length and circumference. The axis of the pipe was coincident with the axis of the water pipe and mixed flow pipe.

The air supply chosen was the 200 psig supply in the Engineering Projects Laboratory. Since the mixing loop was

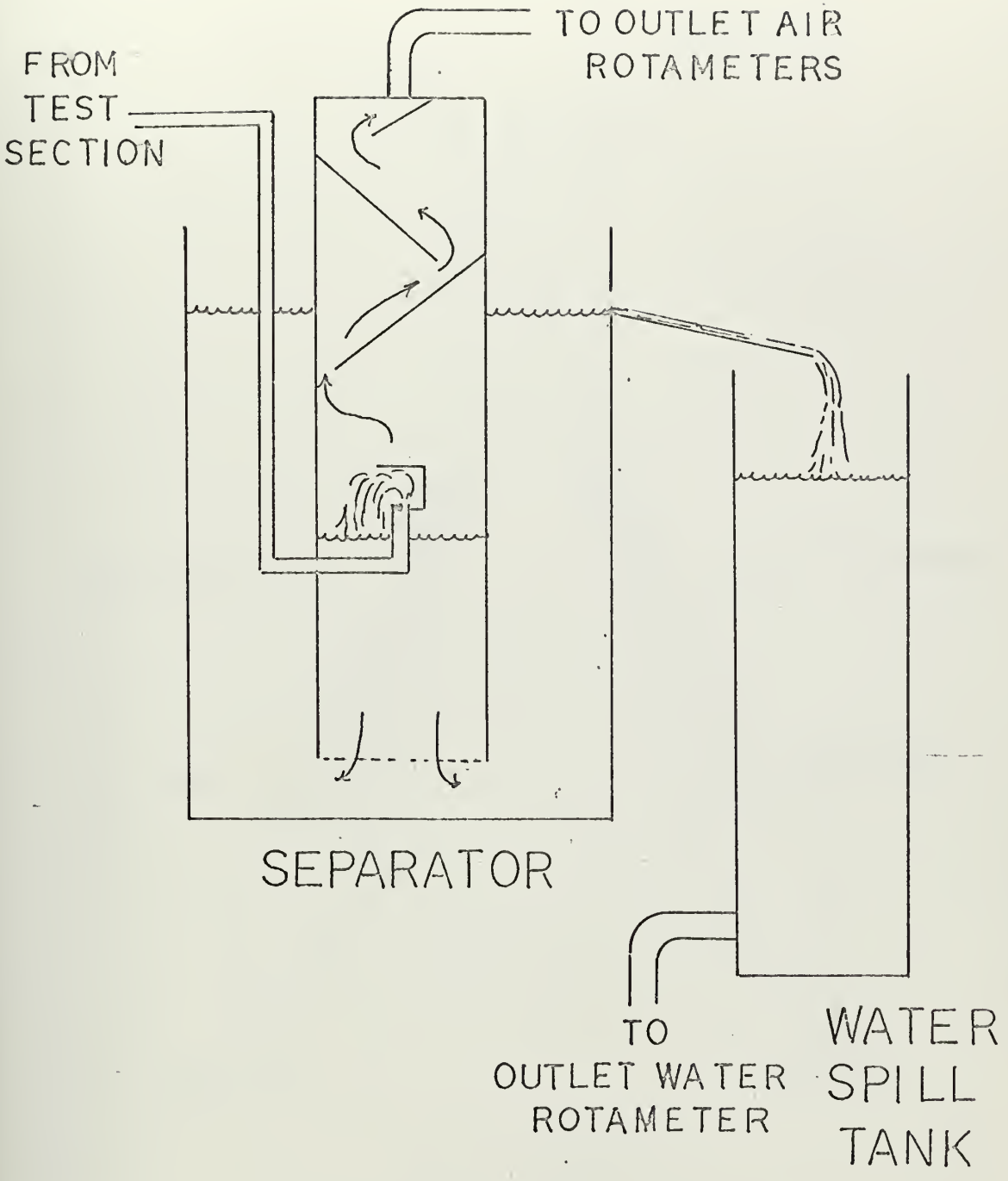

AIR-WATER SEPARATOR

FIGURE 5

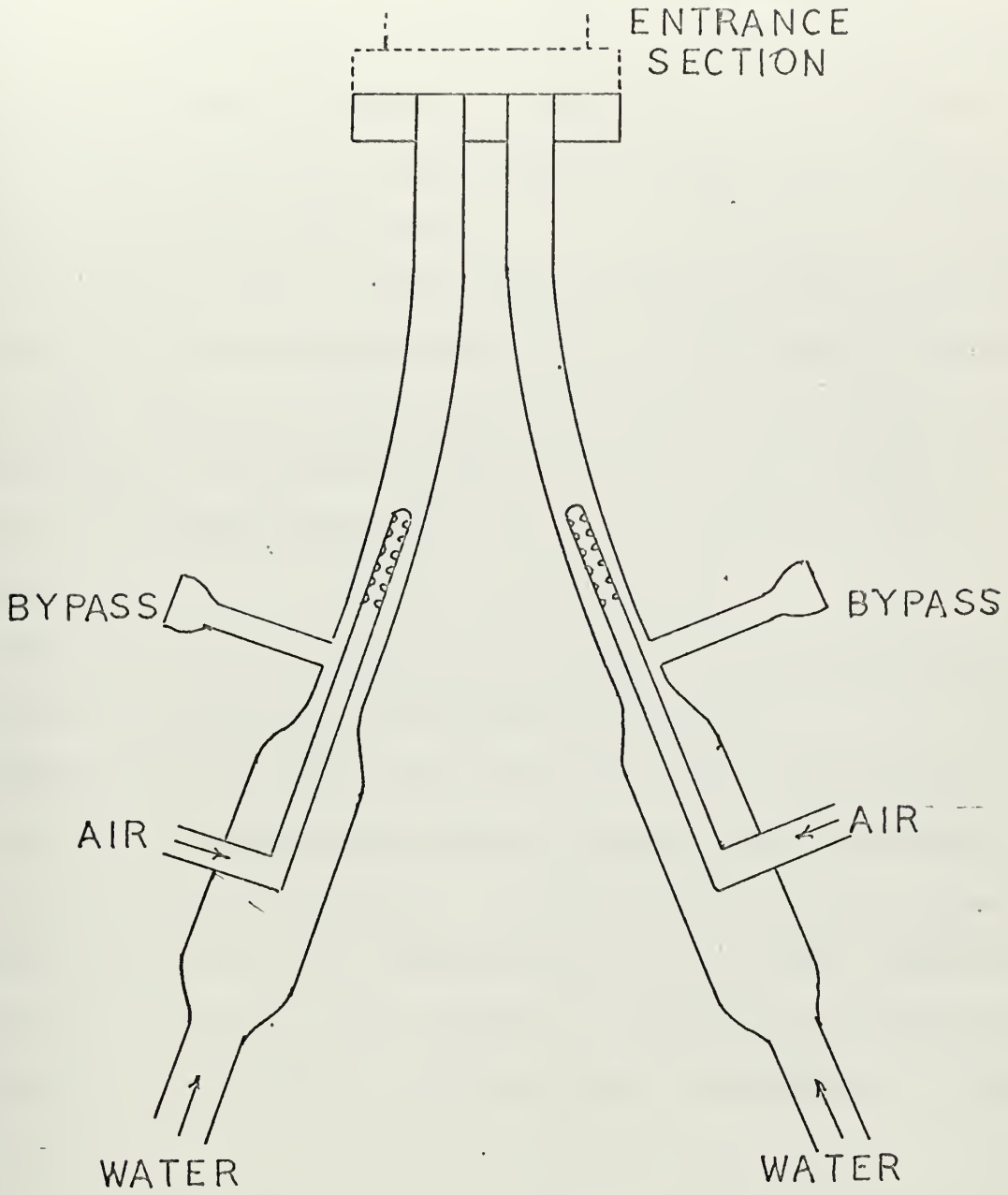

AIR-WATER
MIXING DEVICES

FIGURE 6

the only load on this line, the supply was subject to a minimum of fluctuations. It was found, however, that because of cycling of the compressor, it was necessary to bleed air from the surge tank for proper control by the air pressure regulator at small flow rates.

The water supply (street water pressure) was also subject to some small fluctuations despite use of the regulator and surge tank. Data was taken largely at night to minimize these fluctuations. A water pump may be installed for future operation if higher pressures and less fluctuations are desired.

Filtering was performed with a Cuno Micro-Kleen Filter for air and Fulflo Honeycomb Filter for water.

Thermocouples (L,M) were installed after the exits of the air and water throttle valves to monitor air and water temperatures prior to mixing. It was determined that these temperatures would best represent the air and water conditions in the test section. Only slight air temperature differences between the value before mixing and after separation verified this assumption.

Subchannel Sections

The test section and preceding entrance section were machined in halves from lucite using a special milling cutter. The entrance section and void fraction test section halves were joined with ethelene dichloride (plexiglass cement) to produce a strong joint capable of withstanding the higher

pressures anticipated upon the closing of the void fraction isolation valves. The mixing section halves were joined by bolts and sealed by O ring material.

The entrance section and interchangeable test sections were joined together and to the inlet and exit blocks with rubber gaskets.

The three foot entrance section was preceded by bypass connections (O,P) for use in the void fraction testing configuration. For least disturbance in the flow pattern the bypass connections were placed here rather than just prior to the isolation valves. Thus a three foot long section identical to the test sections in geometry, was provided for establishment of fully developed flow prior to the test sections themselves.

An electric flow regime detector or flow probe (R) was installed in each subchannel. The location of the detector was approximately four inches before the outlet of the entrance section. With the location of the flow probe in the entrance section, flow regime detection was possible for all test section installations. The flow probe itself was manufactured using a 24 gauge stainless steel spring wire with a teflon shield. A silver epoxy paste was painted on the lucite subchannel wall for the wall electrode. Wire leads were imbedded in the subchannel wall underneath the silver epoxy to provide a current path. A detailed description of the electric flow probe installation is given in Appendix B.

Entrance Section

The entrance section was constructed as indicated in Figure 7. A 1/32 inch brass strip was utilized as a subchannel separator, and this strip was sealed in a machined groove in the entrance section wall. It would have been desirable to use a thinner strip in order to model more accurately the conditions in the actual reactor rod bundle. However, two considerations dictated 1/32 inch as the minimum strip thickness. Adequate strength under the possible pressure excursions from valve closing in the void fraction test section required a sufficiently strong strip. Secondly, the sealing of the bottom of the window in the mixing test section required the machining of a groove in the fixed (bottom) portion of the strip to mate with a knife edge in the upper, movable section of the strip. It was this upper, movable portion of the strip which allowed the adjustment of a variable sized window between the two subchannels for determination of turbulent mixing and for complete isolation of the two subchannels from each other when desired.

Since the influence of hydraulic diameter on mixing was also of concern, a "plug" was provided for the right hand subchannel in the entrance and mixing test sections in the form of a brass flat bar machined to specifications and anchored by screws to the subchannel wall. With one set of brass bars in place, both the left and right subchannels were identical. With a second set of brass bars in place, the right subchannel was significantly larger than the left (see Figure 7).

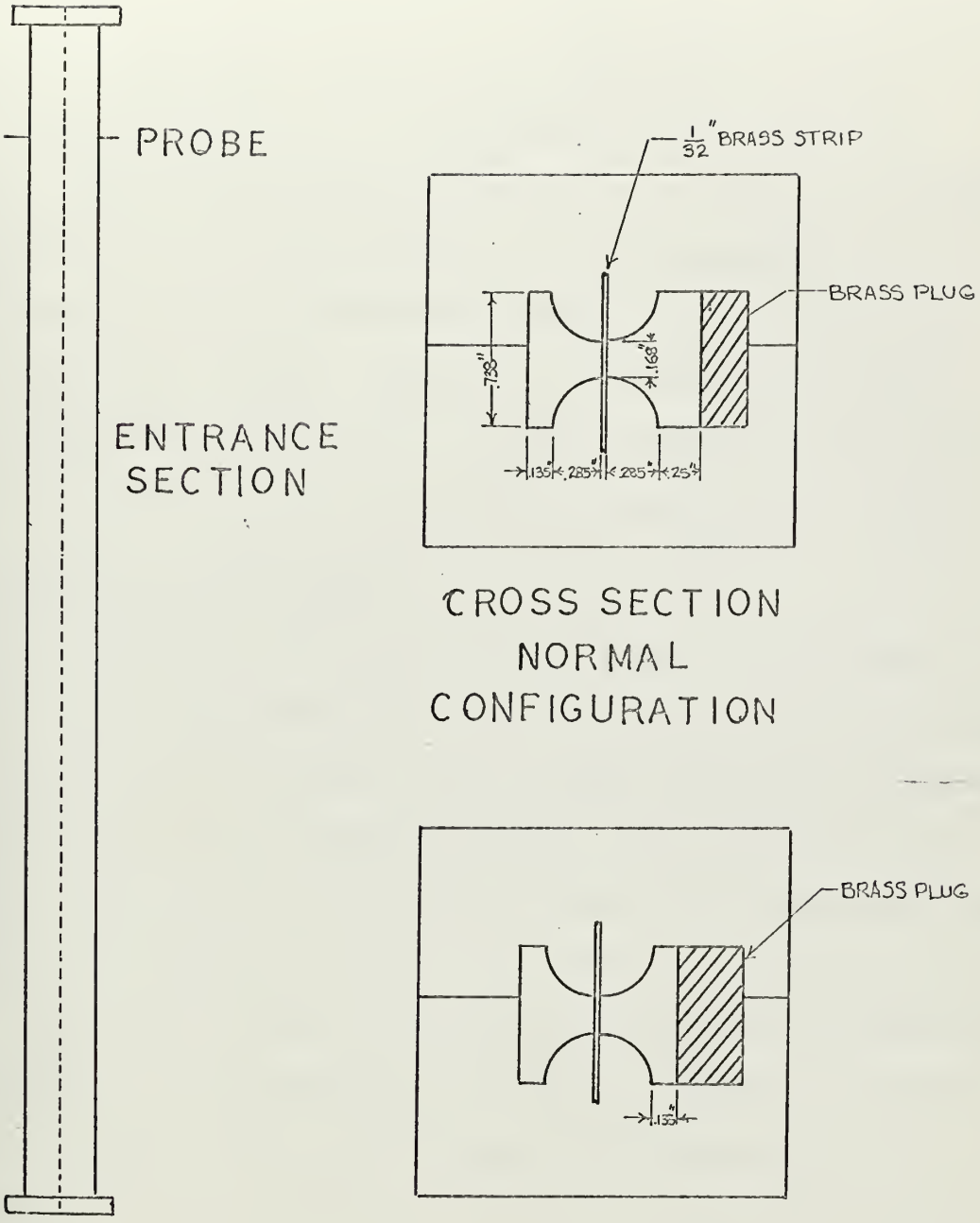
PROBE
ENTRANCE SECTION
1/32" BRASS STRIP
BRASS PLUG
.738"
.168"
.135"
.285"
.285"
.25"
CROSS SECTION
NORMAL
CONFIGURATION
BRASS PLUG
.135"
HYDRAULIC
DIAMETER
MODIFIED
ENTRANCE SECTION

FIGURE 7

Mixing Test Section

The mixing test section was divided into upper and lower sections of three feet and two feet respectively, with a total length of five feet. The bottom of the window was located 2 1/2 feet from the bottom of the mixing test section. The upper brass strip was movable to allow adjustment of the window opening and was withdrawn through a special packing gland in the exit block. A seal on the movable and fixed brass strips was maintained by C clamp pressure on the exterior of the test section. Figure 8 shows the mixing test section.

Void Fraction Test Sections

A photograph of the void fraction apparatus is shown in Figure 9. The construction of the void fraction and entrance section from lucite necessitated a rugged mounting arrangement for the void fraction isolation valves. The void fraction test sections apparatus consisted of two 1 1/4 inch ball valves mounted on a 19 inch x 60 inch x 1/4 inch thick carbon steel plate. The plate in turn was bolted on the Dexion framework. Valve supports were provided by building a boxlike framework of 1/2 inch thick steel and 5/8 inch thick steel bored to accommodate the valve bodies. The valve bodies were machined at the inlet and outlet for brass sleeves which were soldered into the valve inlets and outlets. The sleeves served two purposes: 1) to assist in fastening the valves to the boxlike framework and 2) to permit insertion into the valve ends of

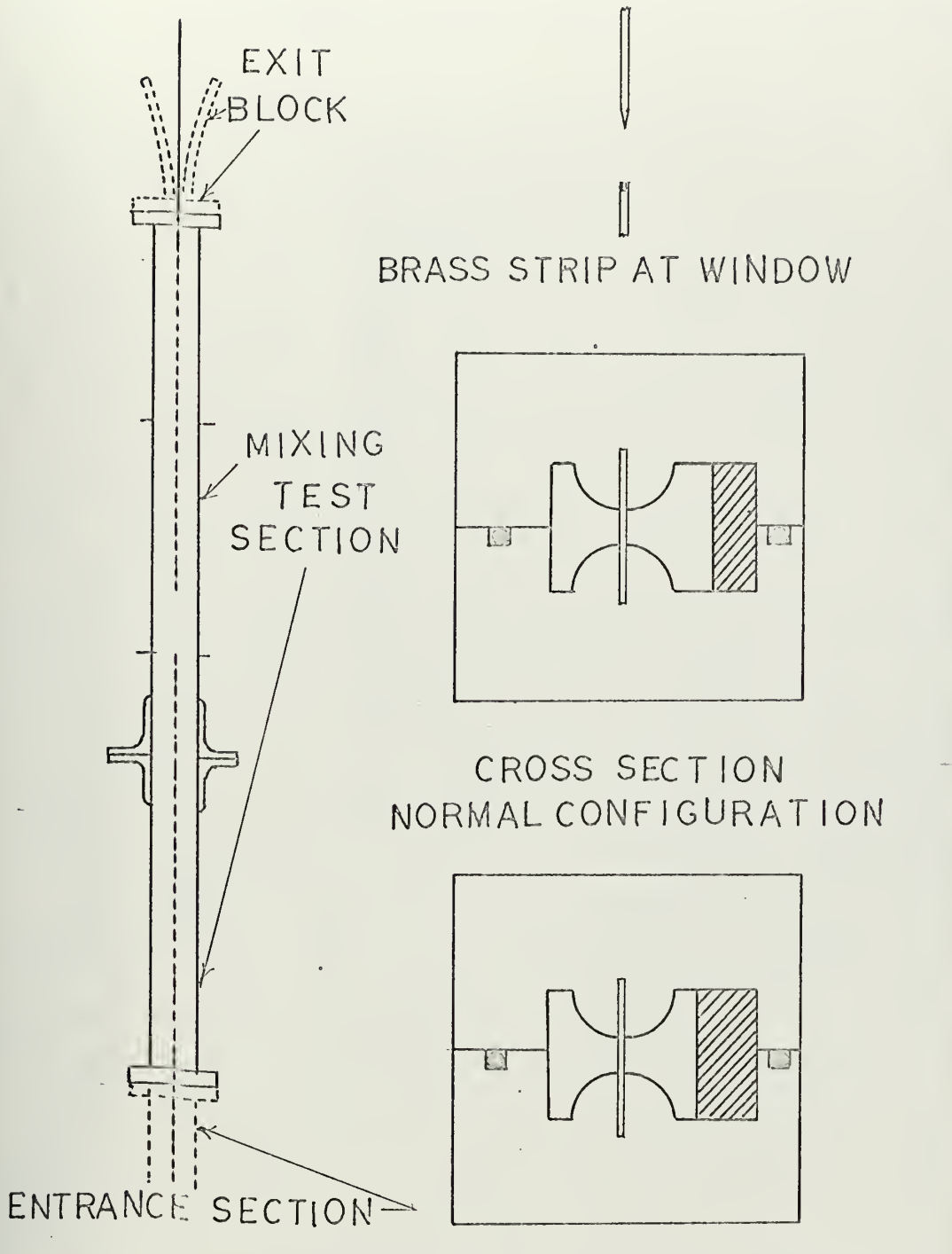

MIXING TEST SECTION

FIGURE 8

Photograph of Void Fraction Apparatus

Figure 9

cylindrical lucite valve inserts with concave ends having the same subchannel geometry as the test section. A similar cylindrical insert with convex ends was provided for each valve ball. Thus the subchannel geometry was maintained throughout the entrance section, isolation valves and void fraction section. The only interruption in the subchannel geometry were the ~.020 inch gaps at the valve balls to preclude hangup of the ball inserts on the Buna N valve seats.

The approximately 48 1/2 inch isolation section between valve balls permitted void fraction determination from approximately 3 - 97%. The 0 - 3 and 97 - 100% range of α was not capable of being read directly because of its being hidden by the valve bodies.

The portion of the test section between the valves was provided with three joints sealed by O rings. Two of the joints were located at the juncture with the valve inserts and the third joint was located in the center of the section. Limitations on the traverse of the milling machine required the test section between the isolation valve inserts to be divided into two, approximately 20 inch long, sections.

The void fraction test section apparatus consisted of a left subchannel and a right subchannel section, each capable of being installed while the main steel mounting plate was in place on the Dexion structure. Thus, there were interchangable valve inserts, valve ball inserts and void fraction isolation sections for both the left and right hand subchannels. A

photograph of these pieces is shown in Figure 10. Figure 11 shows the valve ball insert in place.

Void fraction divisions from 3 - 97.5% were scribed on the front only of the isolation sections by use of a milling machine. Visual error in reading void fractions due to refraction was found to be minimal since the meniscus provided a gauge for determining when the line of sight to the air-water interface was above or below the line of sight perpendicular to the interface.

Pressure taps for the pressure level and pressure drop determination were installed three feet apart in the isolation section of the void fraction test sections. Pressure transducer and transducer readouts were utilized. This instrumentation permitted accurate determination of the pressure level and pressure drop.

The valve closure device selected was an air piston operated mechanical linkage actuated by an electric solenoid simultaneously with a similarly operated bypass valve. The main isolation valves were mechanically linked by a steel operating rod and operated by a single air piston and cylinder. The bypass valve was operated by a similar linkage but with a separate air piston because of the large distance from the test section to the bypass valve. The bypass valve (and operating mechanism) was mounted on a separate Dexion and wood framework on the lower level.

Each air operated piston and cylinder was actuated by separate solenoids connected electrically in parallel.

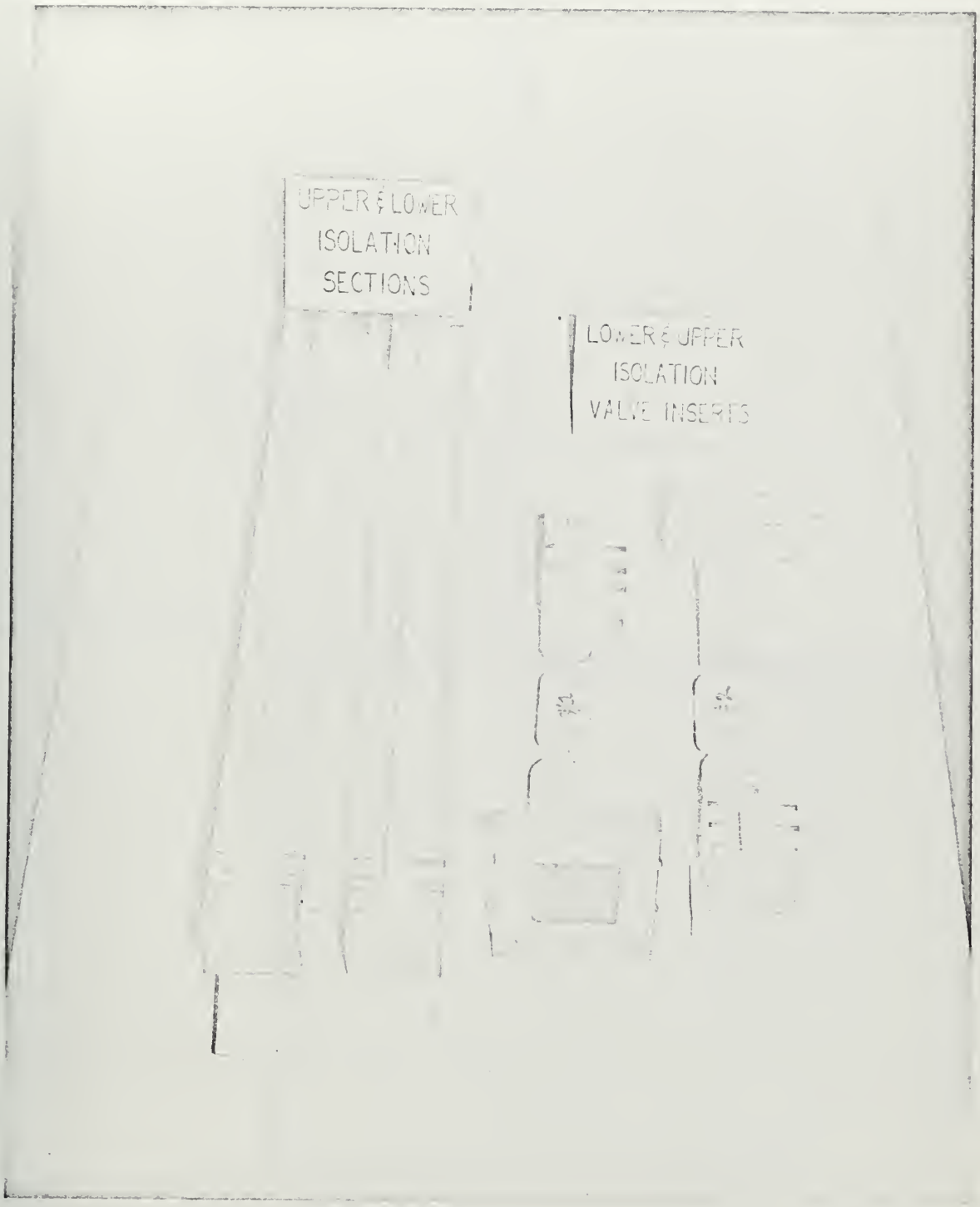

Photograph of Void Fraction Isolation Test Sections and Valve Inserts--Left Subchannel

Figure 10

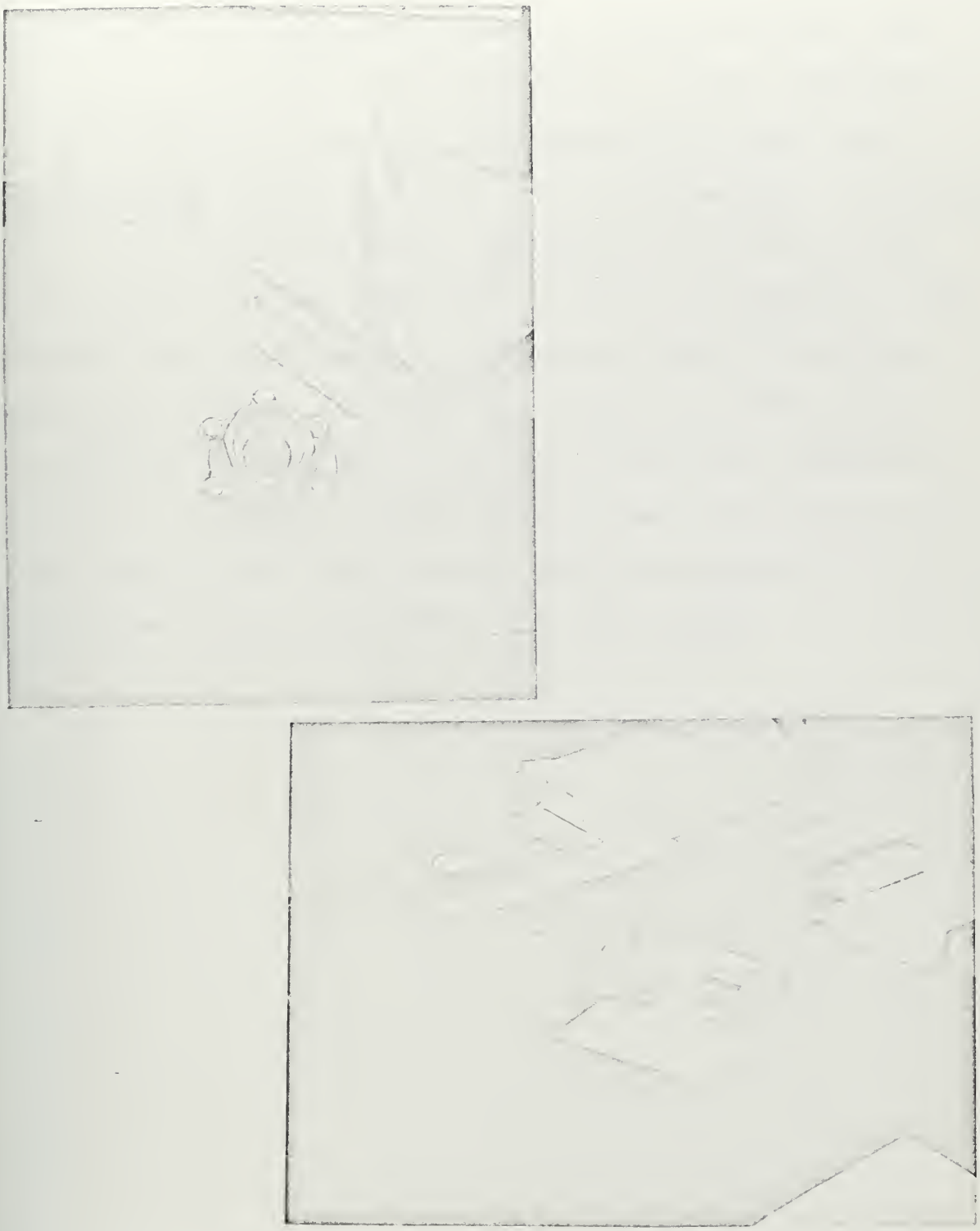

Photographs of Valve Ball Insert in Valve and Valve Insert Assembly

Figure 11

Actuation of the solenoids closed the isolation valves and simultaneously opened the bypass valve. Careful adjustment of air operating pressure to the separate cylinders gave a reliable simultaneous operation in 70 milliseconds. Preliminary calculations using the Wallis correlation (4) for air and water showed this to effectively isolate the section in ~30% of the transit time for the gas phase at 80% void fraction and $G_{water} = 1 \times 10^6$ lb/ft^{2}hr. The channel was effectively isolated in 1/8 turn of the isolation valves and completely isolated in 1/4 turn. Valve closing times were monitored on a dual beam storage oscilloscope using an electrical circuit with potentiometers mounted on the valve stems.

CHAPTER IV

Procedure

The right subchannel void fraction test section complete with valves and inserts was mounted first above the right hand subchannel of the entrance section. By so doing, the left subchannel of the entrance section was blocked off. The bypass valve was connected to the right subchannel bypass connection.

The inlet water flow rate was set at predetermined superficial liquid mass velocities matching the range of mass velocities in a typical boiling water reactor. Six superficial mass velocities ranging from 0.5×10^6 to 1.0×10^6 $LB_m/HR\ FT^2$ (with a 0.1×10^6 increment) were investigated.

For each liquid mass velocity, the air flow rate, monitored at the exit of the separators, was varied throughout the flow range of the air flow meter bank. Several void fraction readings (at least three) were taken at each air flow rate and from this, an average void fraction was determined. It was found that in the bubbly flow regime there was little scatter in the data, while in the slug flow regime as many as five or six trapped samples were necessary to achieve a smooth void fraction curve. Under identical conditions individual void fraction readings varied by as much as 8% in the slug flow regime.

For each flow condition air temperature was recorded both prior to mixing with water and after separation. Water temperature was monitored prior to mixing only.

Both pressure level and pressure drop in the test section were recorded for each point. A low-pass filter was provided between the Δp transducer readout and the vacuum tube voltmeter to dampen the effect of the pressure drop oscillations in the slug flow regime.

The electrical conductivity probe and visual observations were used to determine the flow regime boundaries. Polaroid photographs of the flow probe traces were taken for permanent record of the flow conditions. Several representative photographs are shown in Appendix B, Figure B-2. These photographs enable the determination of typical slug lengths.

It was found that the design of the separators was limiting the void fraction to about 65%. At these high air flow rates, increased pressure drop in the exit piping and exit air rotameters caused a buildup of pressure in the inner, inverted "can" of the separators. This pressure exceeded the hydrostatic pressure maintained by the water in the outer drum and resulted in escape of the air from the bottom of the inner can. Redesign or modification of the separators will be necessary to reach higher void fractions.

When the required data had been obtained for the right hand channel, the corresponding void fraction test section was removed and the operations were repeated for the left subchannel.

Alteration of the valve closing speed over a range of 100-160 milliseconds showed no change in the average void fraction measured for typical conditions in the slug flow

regime. Although initial valve closure times were of the order of 70 milliseconds, an average of 100 milliseconds was maintained throughout the data taking period.

The instrumentation was calibrated as follows:

a) air rotameters: initial calibration with known air volume flow rates using a gasometer

b) water rotameters: initial calibration with known water flow rates using a weigh tank

c) pressure level transducer: calibration prior to each data taking run using a mercury manometer (normally daily)

d) Δp transducer: electrical calibration prior to each data taking run (normally daily)

e) air and water thermocouples: no calibration

It is emphasized that throughout the range of flow conditions covered by this experiment, no attempt was made to maintain pressure level constant at any location in the test section.

CHAPTER V

Results

The experimental results of this thesis are presented graphically in this chapter for the highest and lowest values of superficial liquid mass velocity (1.0×10^6 and 0.5×10^6 $LB_m/HR\ FT^2$).

Data are presented in tabular form for these superficial mass velocities and intermediate values in Appendix C.

Void fraction data are plotted against W_g, the air mass flow rate, which is directly proportional to quality for the low air mass flow rates investigated. Flow regime boundaries are indicated on these graphs. Figures 12-15 show these data and compare them to correlations by Griffith (12), Lockhart-Martinelli (5) and Cravarolo and Hassid (13). The Griffith prediction applies to the slug flow regime only and is plotted for a round tube having the same hydraulic diameter. The Lockhart-Martinelli correlation was developed for air and water and many other liquids in round tubes and horizontal adiabatic flow. Cravarolo and Hassid's data was obtained for argon and water or ethyl alcohol in several geometries: tubes, annuli, and a seven rod bundle in a circular shroud.

The pressure gradient was plotted against void fraction, since this information is considered to be of interest in establishing the proper conditions for the forthcoming mixing experiments. A prediction by the Lockhart-Martinelli correlation for total pressure gradient versus void fraction, is

included for comparison. Measured local conditions (i.e., pressure level and temperature at the level corresponding to the window location in the mixing test section) were used in the Lockhart-Martinelli correlation. It is possible, however, to predict void fraction and total pressure drop using this correlation without knowledge of the pressure at the window location. This could be done by iterative calculations of pressure gradient and void fraction. Pressure gradient data is shown in graphical form in Figures 16-19.

Average slip ratio is shown in Figures 20-23. The Marchaterre-Hoglund correlation (14) for slip is shown in these figures for comparison. This correlation was developed to predict velocity ratios in vertical channels of boiling water reactors. These researchers investigate several geometries in formulating their correlation (which makes no distinction for differing geometry). Both adiabatic and diabatic cases were studied for steam and water in rectangular and circular channels. Air-water experiments were conducted in rectangular channels only. Rod bundle geometries were not investigated.

Average gas velocity, $\bar{V}_g = \frac{\langle j_g \rangle}{\langle \alpha \rangle}$, was plotted against average volumetric flux density, $\langle j \rangle$, in Figures 24-27, in the form set forth by Zuber and Findlay (9). These plots permitted the determination of C_o, the velocity and concentration distribution parameter, and $\bar{V}_{gj}$, the weighted average gas drift velocity. In all cases investigated, $\bar{V}_{gj}$ was found

to be very small, less than 1 FT/SEC. Values of C_o of about 1.25 were obtained for a superficial liquid mass velocity, G_f, of 0.5×10^6 in both subchannels. For the higher mass velocity, $G_f = 1.0 \times 10^6$, a value of about 1.20 for C_o was obtained.

Intermediate superficial mass velocities for the left subchannel will be investigated in subsequent work.

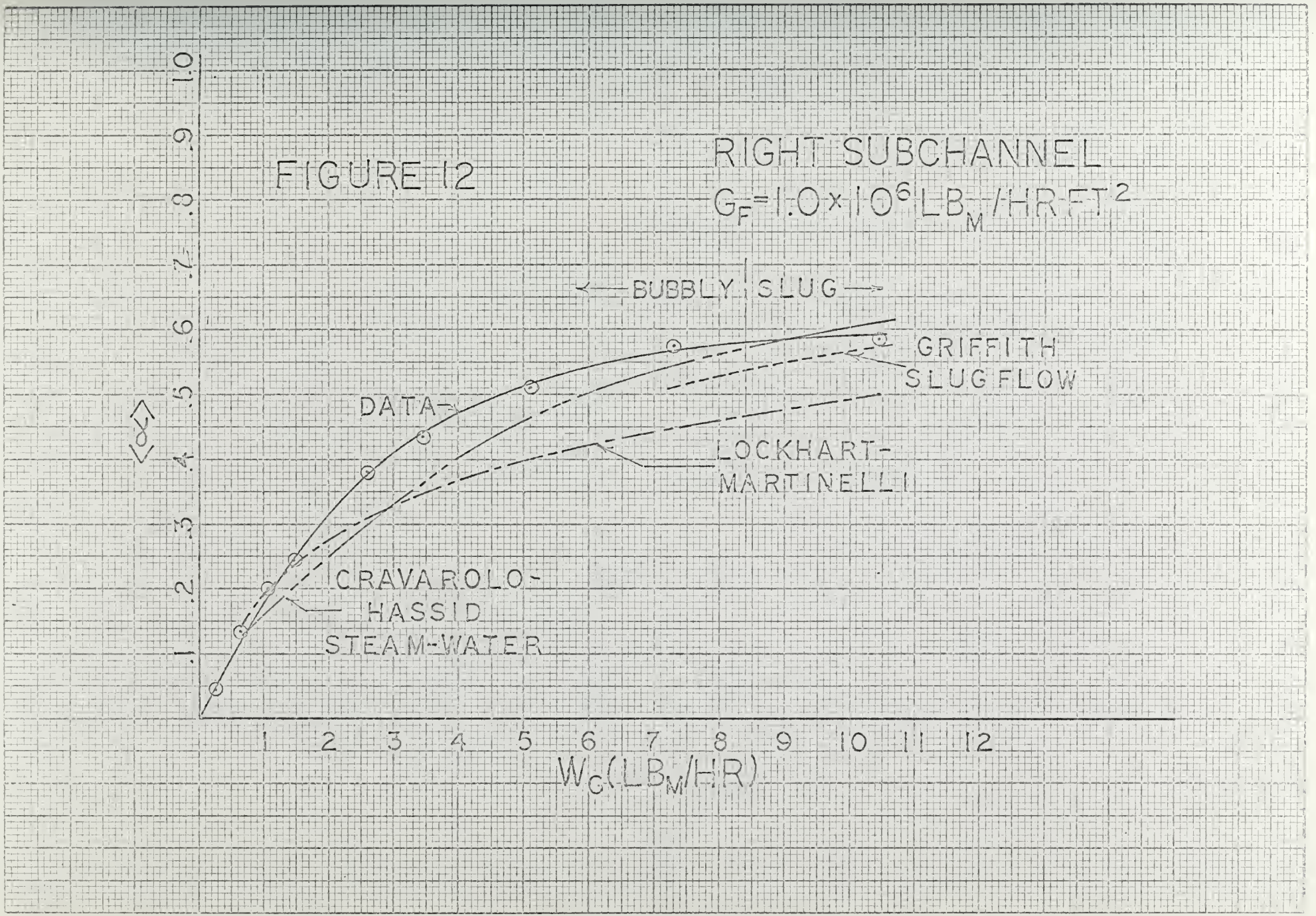
FIGURE 12
RIGHT SUBCHANNEL
$G_F = 1.0 \times 10^6$ LB$_M$/HR FT^2
BUBBLY
SLUG
GRIFFITH SLUG FLOW
DATA
LOCKHART-MARTINELLI
CRAVAROLO-HASSID STEAM-WATER
$\langle \alpha \rangle$
.1
.2
.3
.4
.5
.6
.7
.8
.9
1.0
1 2 3 4 5 6 7 8 9 10 11 12
W_G(LB$_M$/HR)

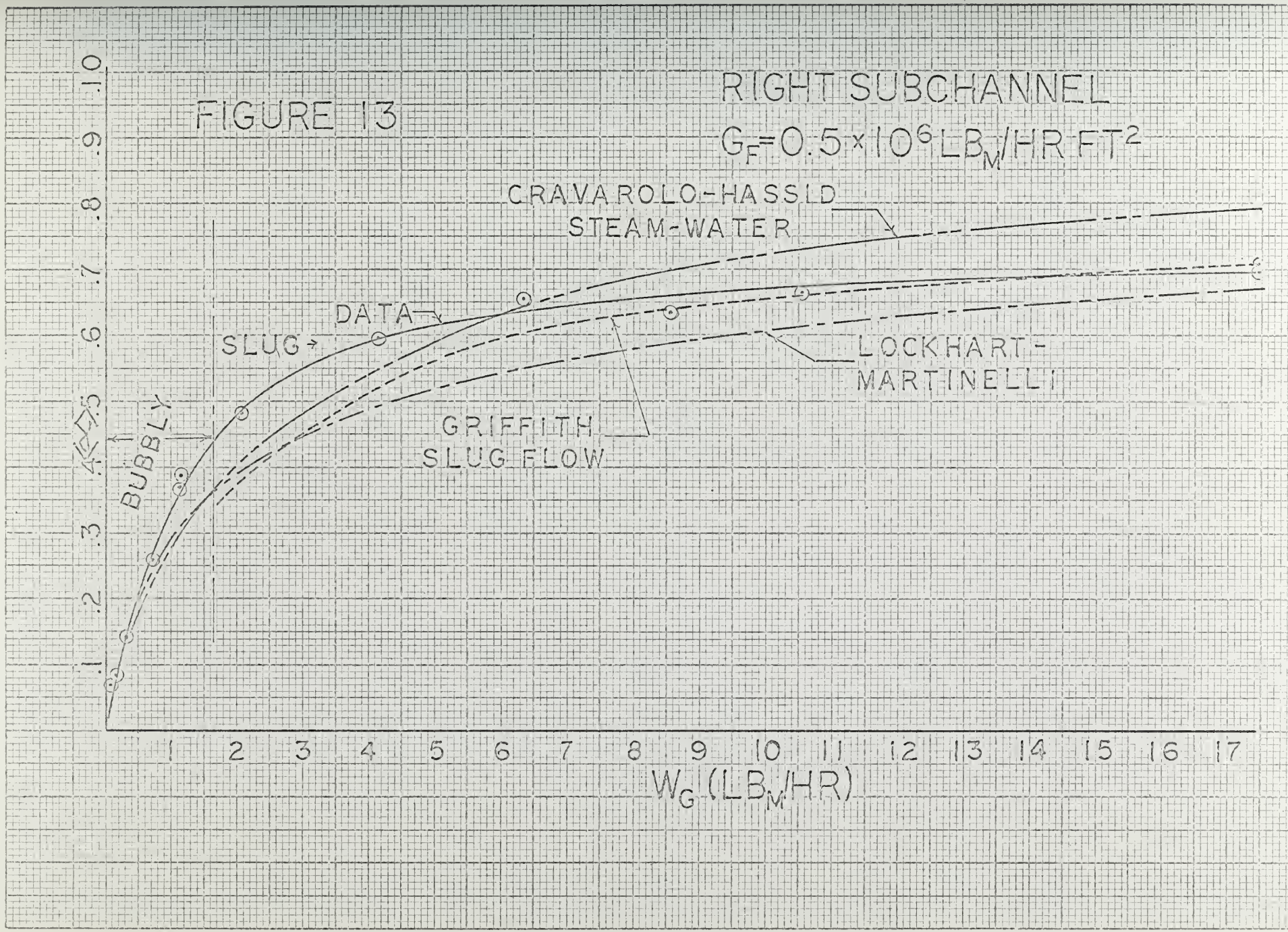
FIGURE 13
RIGHT SUBCHANNEL
$G_F = 0.5 \times 10^6$ LB$_M$/HR FT^2
CRAVAROLO-HASSID
STEAM-WATER
DATA
SLUG
BUBBLY
LOCKHART-
MARTINELLI
GRIFFITH
SLUG FLOW
1 2 3 4 5 6 7 8 9 10
1 2 3 4 5 6 7 8 9 10 11 12 13 14 15 16 17
W_G (LB$_M$/HR)

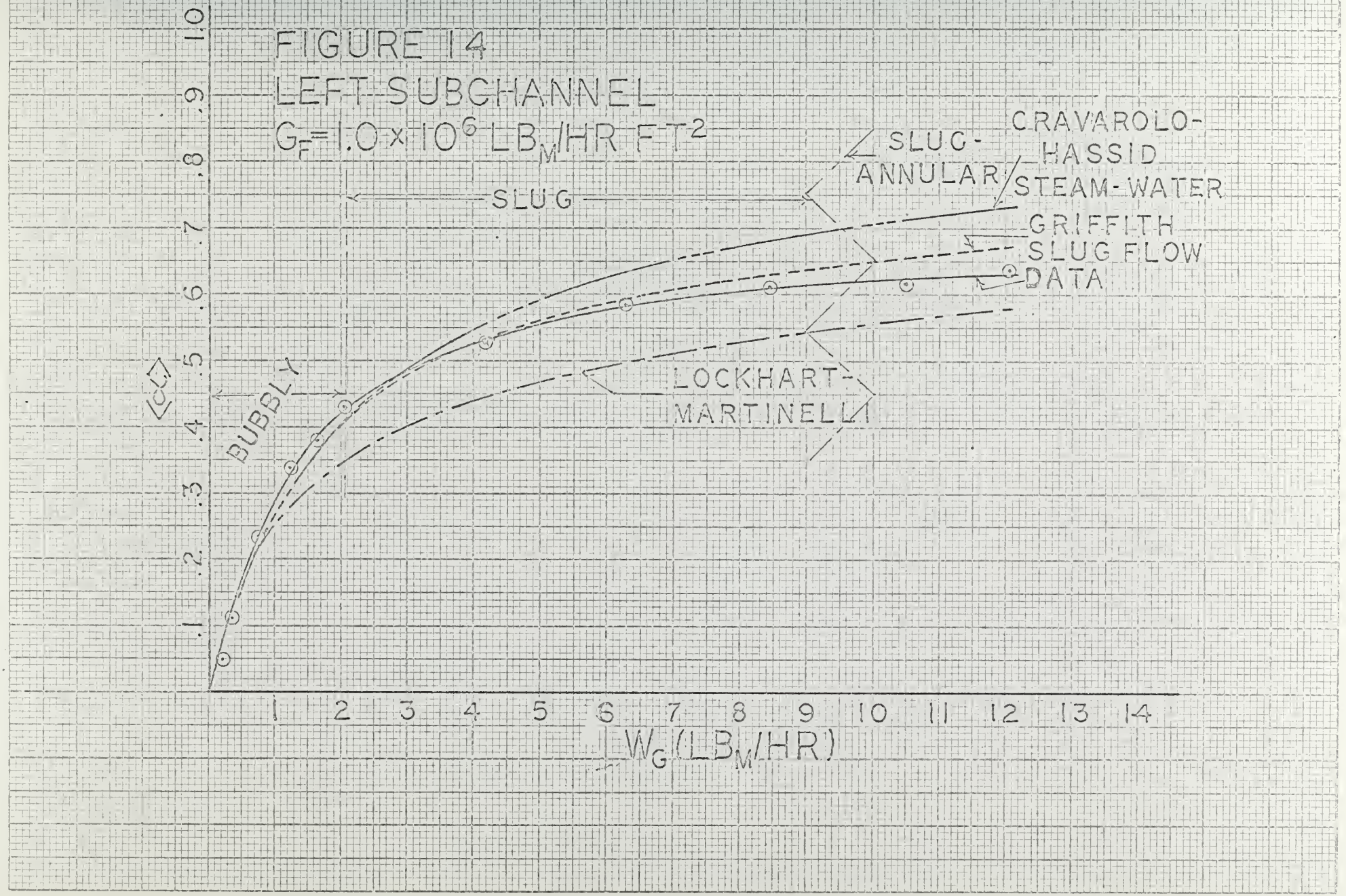
FIGURE 14
LEFT SUBCHANNEL
$G_F = 1.0 \times 10^6$ LB$_M$/HR FT^2
SLUG
SLUG-ANNULAR
CRAVAROLO-HASSID STEAM-WATER
GRIFFITH SLUG FLOW
DATA
LOCKHART-MARTINELLI
BUBBLY
⟨C⟩
.1 .2 .3 .4 .5 .6 .7 .8 .9 1.0
1 2 3 4 5 6 7 8 9 10 11 12 13 14
W_G (LB$_M$/HR)

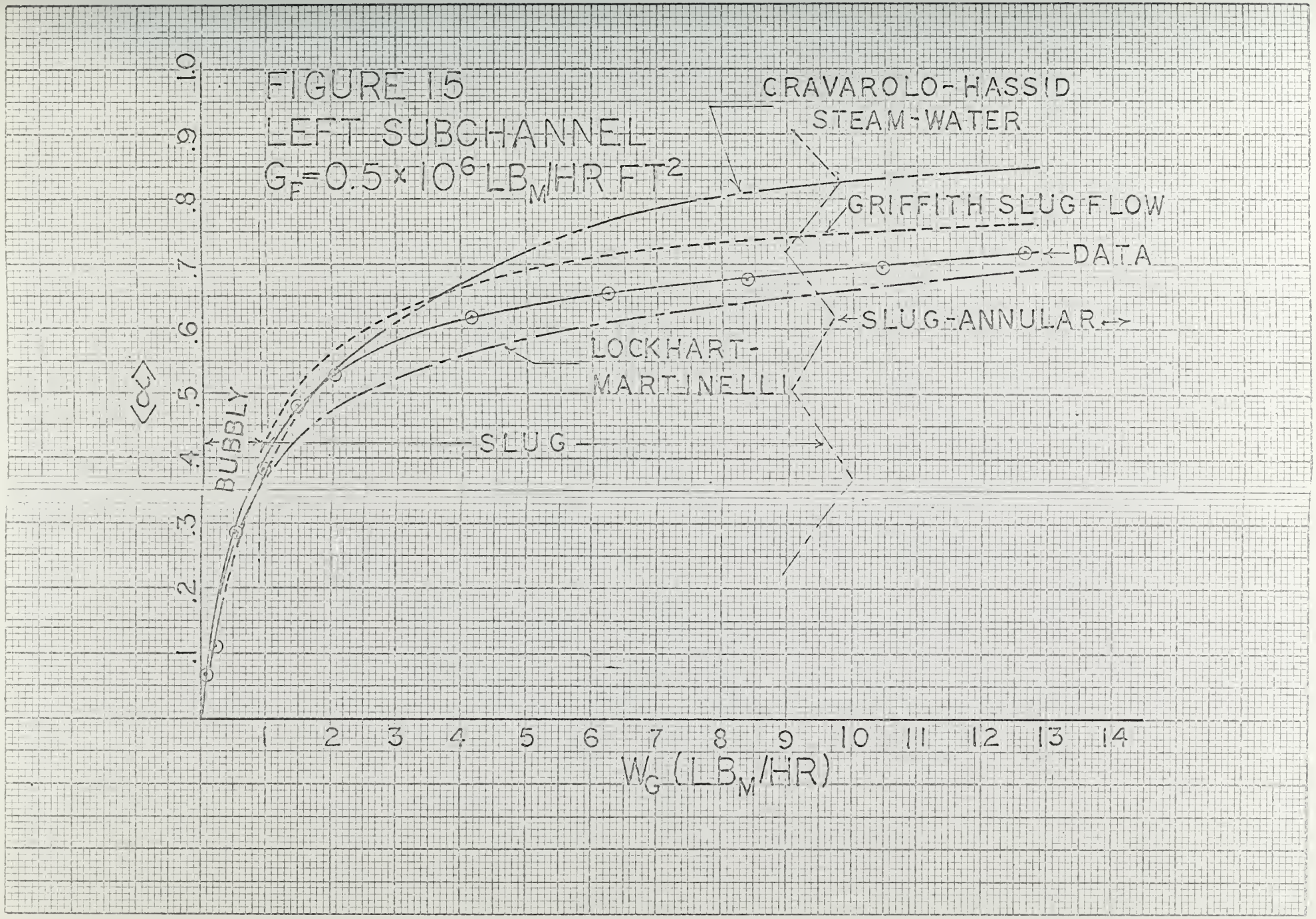
FIGURE 15
LEFT SUBCHANNEL
$G_F = 0.5 \times 10^6$ LB$_M$/HR FT^2
CRAVAROLO-HASSID
STEAM-WATER
GRIFFITH SLUG FLOW
DATA
SLUG-ANNULAR
LOCKHART-
MARTINELLI
SLUG
BUBBLY
⟨C⟩
.1
.2
.3
.4
.5
.6
.7
.8
.9
1.0
1
2
3
4
5
6
7
8
9
10
11
12
13
14
W_G (LB$_M$/HR)

FIGURE 16
RIGHT SUBCHANNEL
$G_F = 1.0 \times 10^6 LB_M/HR\,FT^2$
$\left(\frac{dp}{dz}\right)_{TOTAL}$ (PSI/FT)
LOCKHART-MARTINELLI
DATA
$\langle x \rangle$
.1
.2
.3
.4
.5
.6
.7
.8
1.
2.
3.
4.
5.
6.
7.

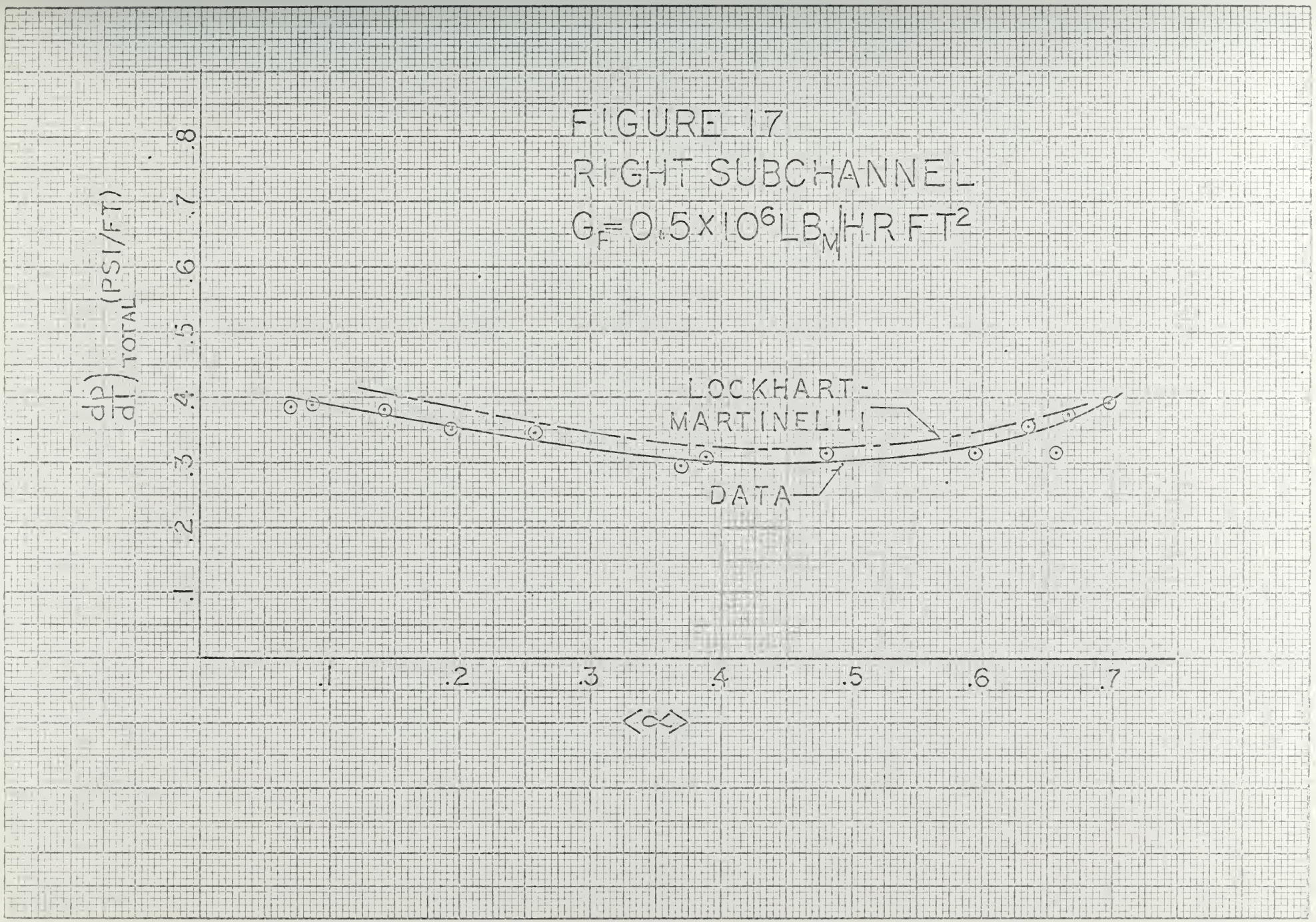
FIGURE 17
RIGHT SUBCHANNEL
$G_F = 0.5 \times 10^6 LB_M/HR\,FT^2$
$\left(\frac{dp}{dl}\right)_{TOTAL}$ (PSI/FT)
.1
.2
.3
.4
.5
.6
.7
.8
LOCKHART-
MARTINELLI
DATA
.1
.2
.3
.4
.5
.6
.7
$\langle \alpha \rangle$

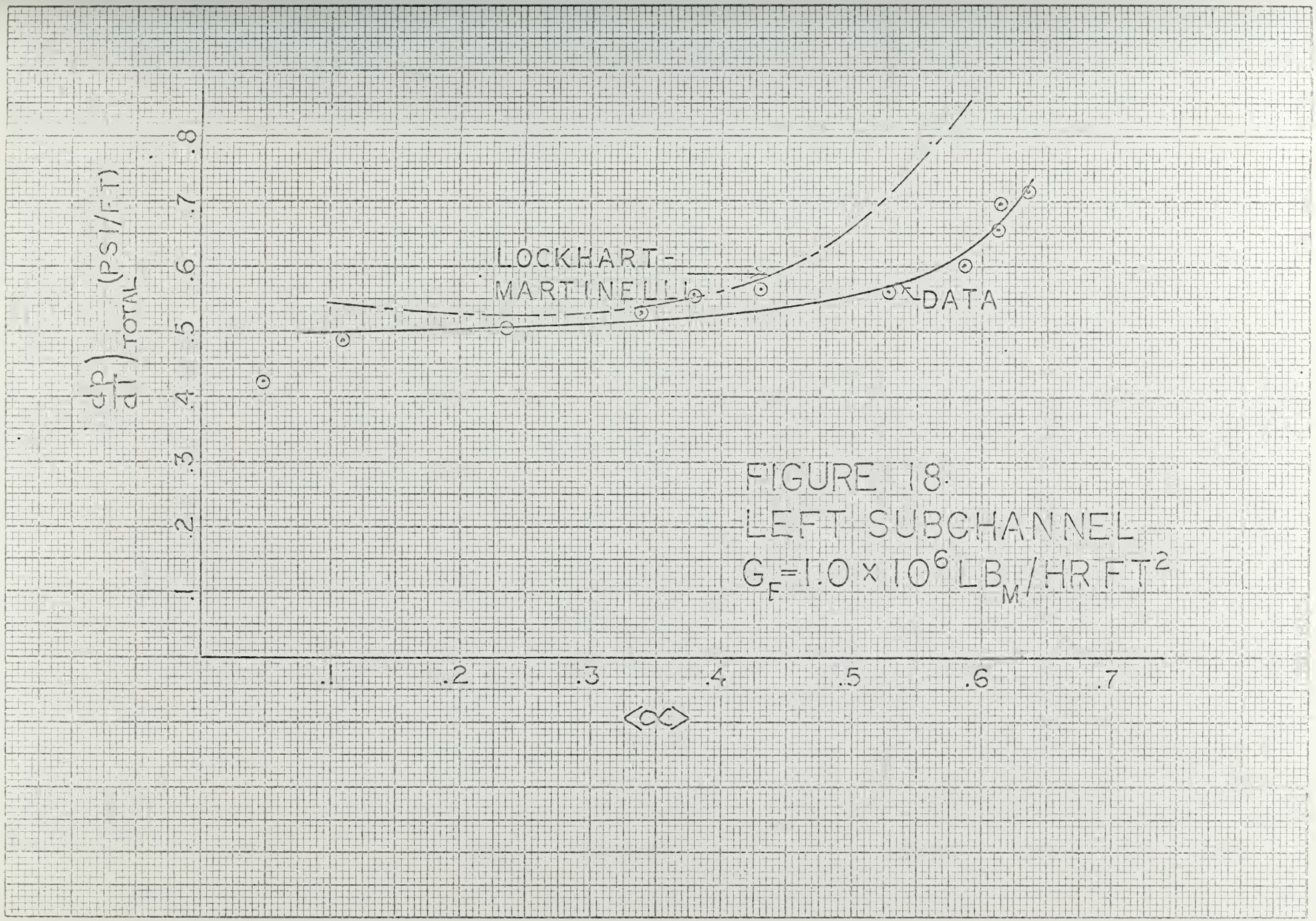

FIGURE 18.
LEFT SUBCHANNEL
$G_F = 1.0 \times 10^6$ LB$_M$/HR FT^2

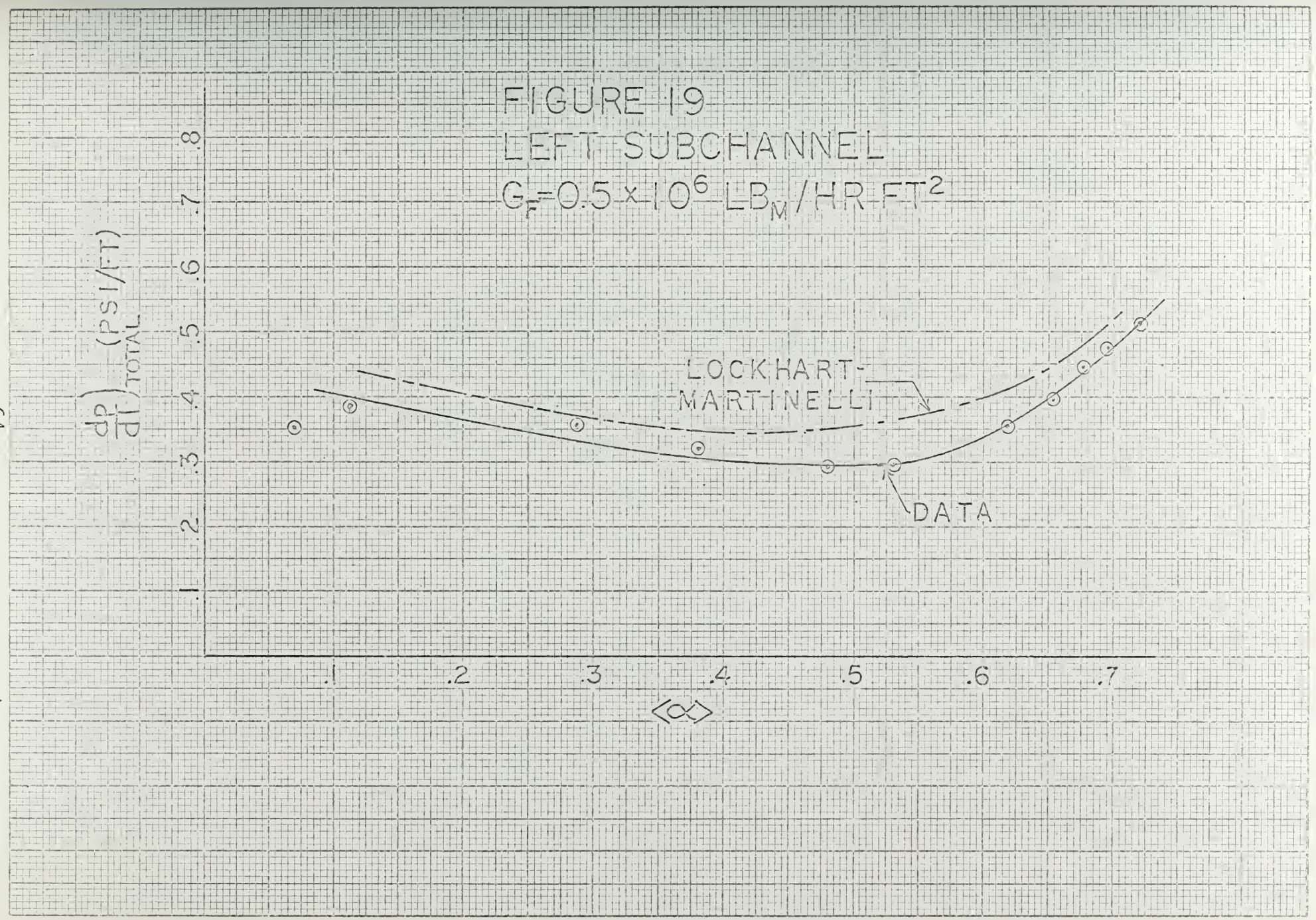
FIGURE 19
LEFT SUBCHANNEL
$G_F = 0.5 \times 10^6$ LB$_M$/HR FT^2
$\left(\frac{dp}{dt}\right)_{TOTAL}$ (PSI/FT)
.1
.2
.3
.4
.5
.6
.7
.8
LOCKHART-MARTINELLI
DATA
.1
.2
.3
.4
.5
.6
.7
⟨α⟩

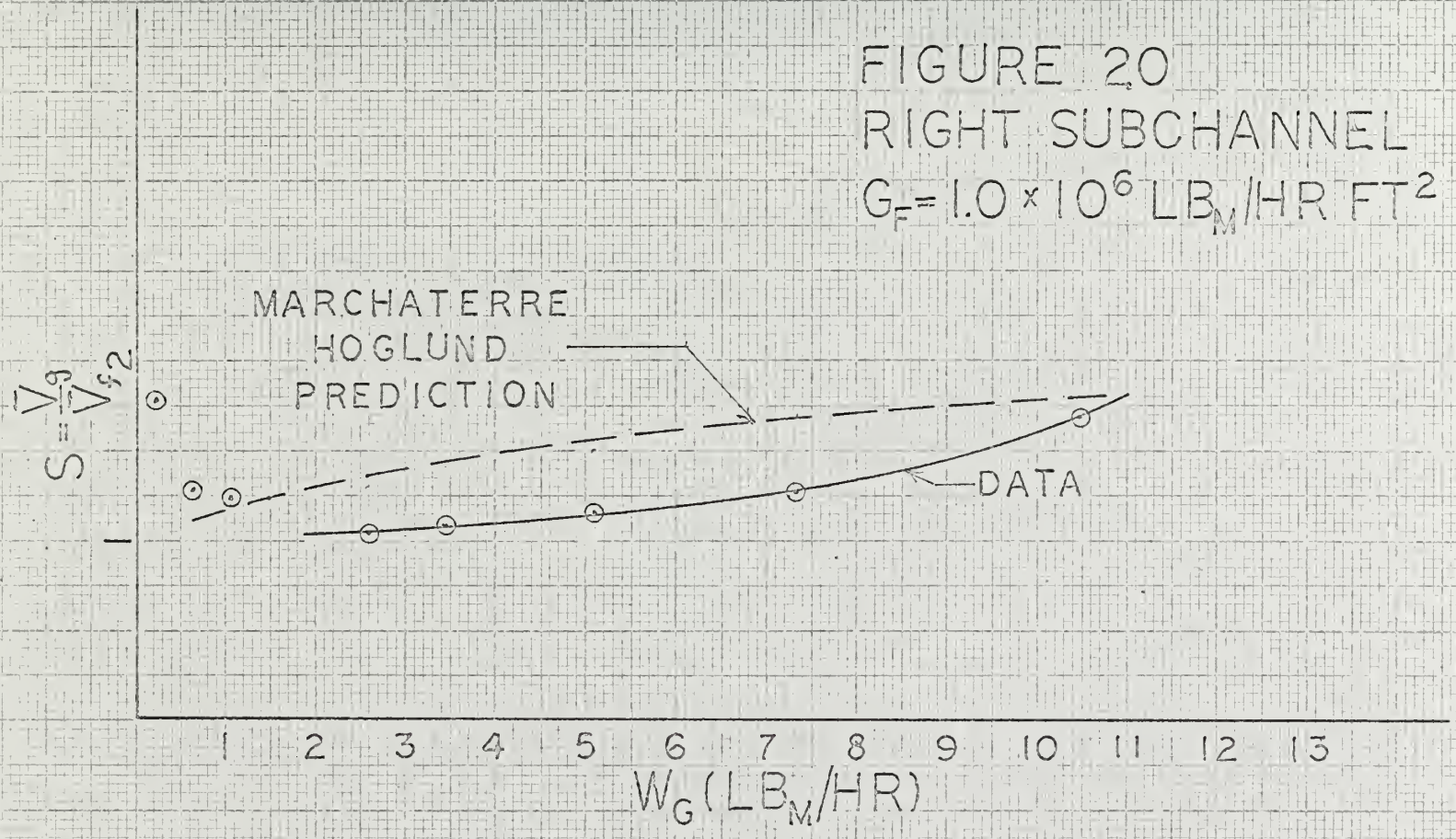
FIGURE 20
RIGHT SUBCHANNEL
$G_F = 1.0 \times 10^6$ LB$_M$/HR FT^2
MARCHATERRE
HOGLUND
PREDICTION
DATA
$S = \frac{V_g}{V_{f2}}$
1
1 2 3 4 5 6 7 8 9 10 11 12 13
W_G (LB$_M$/HR)

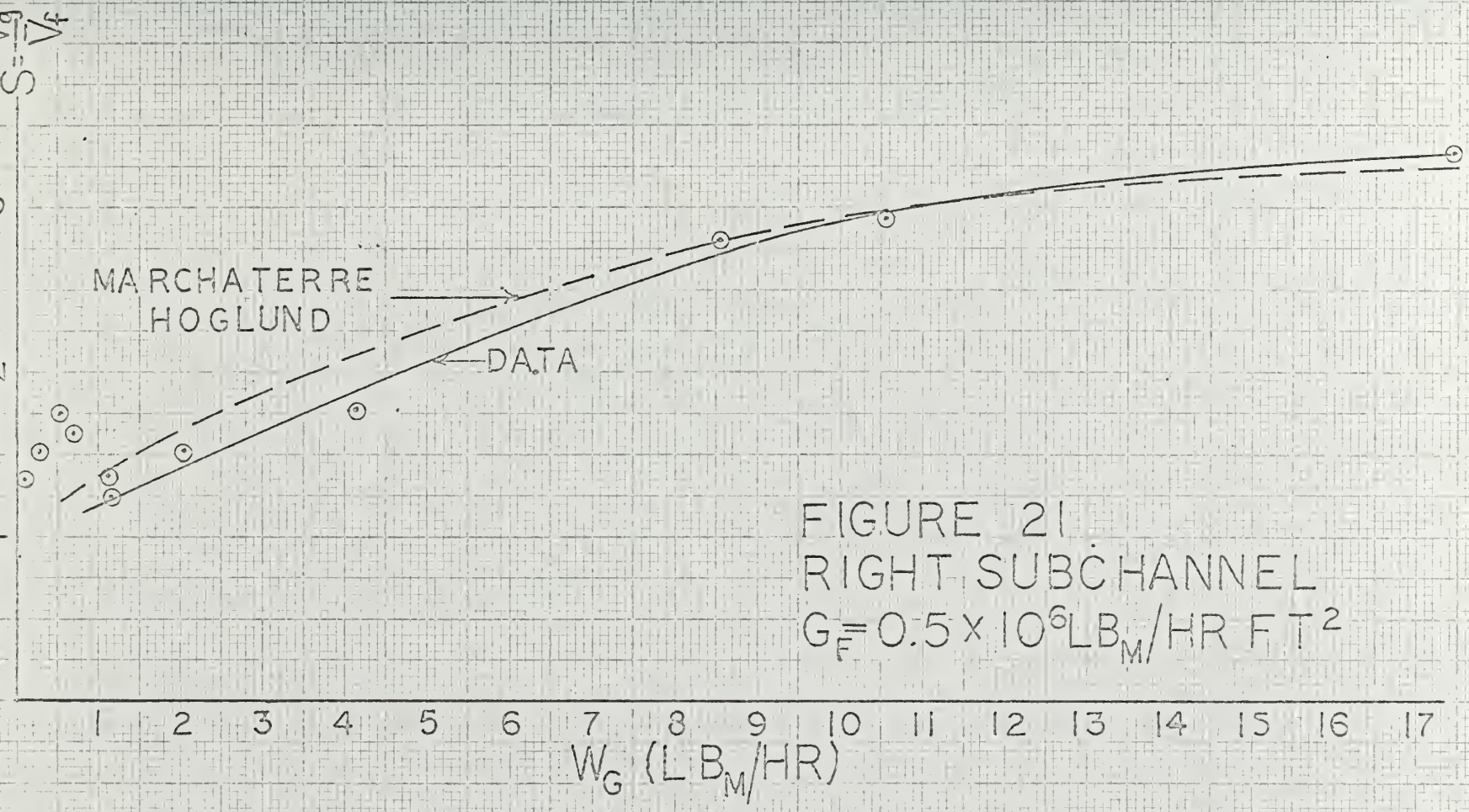

FIGURE 21
RIGHT SUBCHANNEL
$G_F = 0.5 \times 10^6$ LB$_M$/HR FT^2

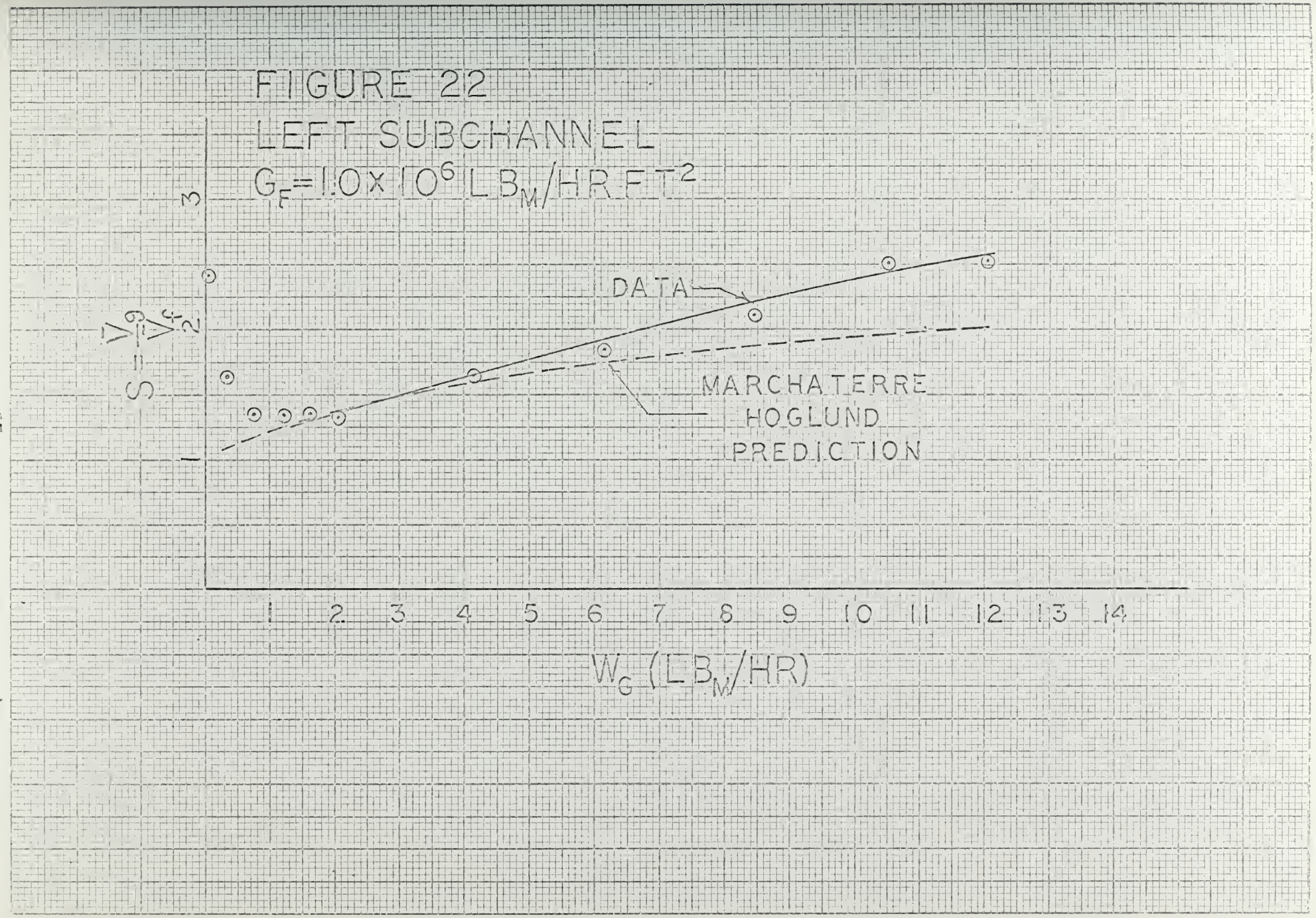
FIGURE 22
LEFT SUBCHANNEL
$G_F = 1.0 \times 10^6$ LB$_M$/HR FT^2
$S = V_g / V_{s2}$
3
1
DATA
MARCHATERRE
HOGLUND
PREDICTION
1 2 3 4 5 6 7 8 9 10 11 12 13 14
W_G (LB$_M$/HR)

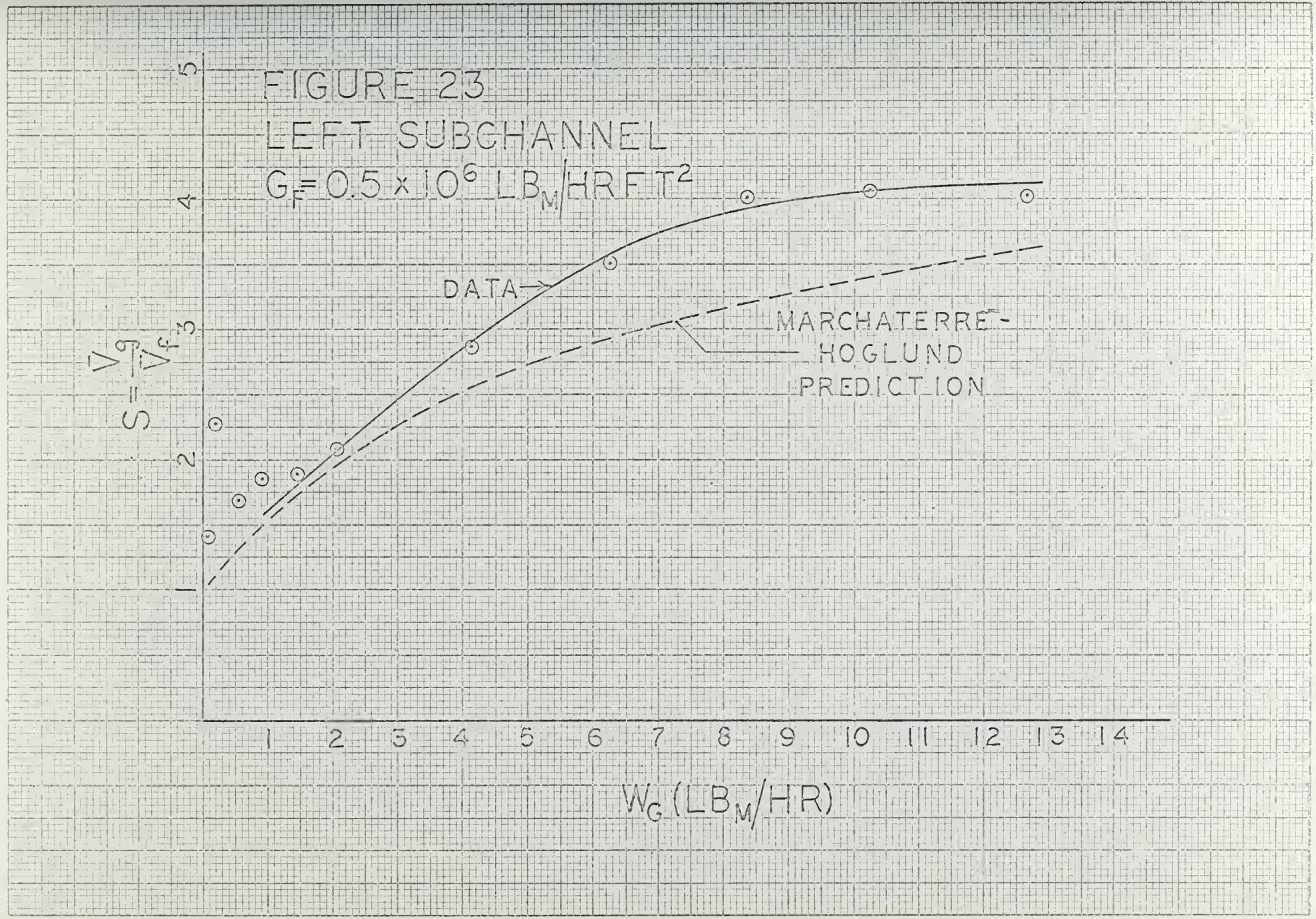
FIGURE 23
LEFT SUBCHANNEL
$G_F = 0.5 \times 10^6$ LB$_M$/HR FT^2
DATA
MARCHATERRE-HOGLUND PREDICTION
$S = V_g / V_f$
1
2
3
4
5
1 2 3 4 5 6 7 8 9 10 11 12 13 14
W_G (LB$_M$/HR)

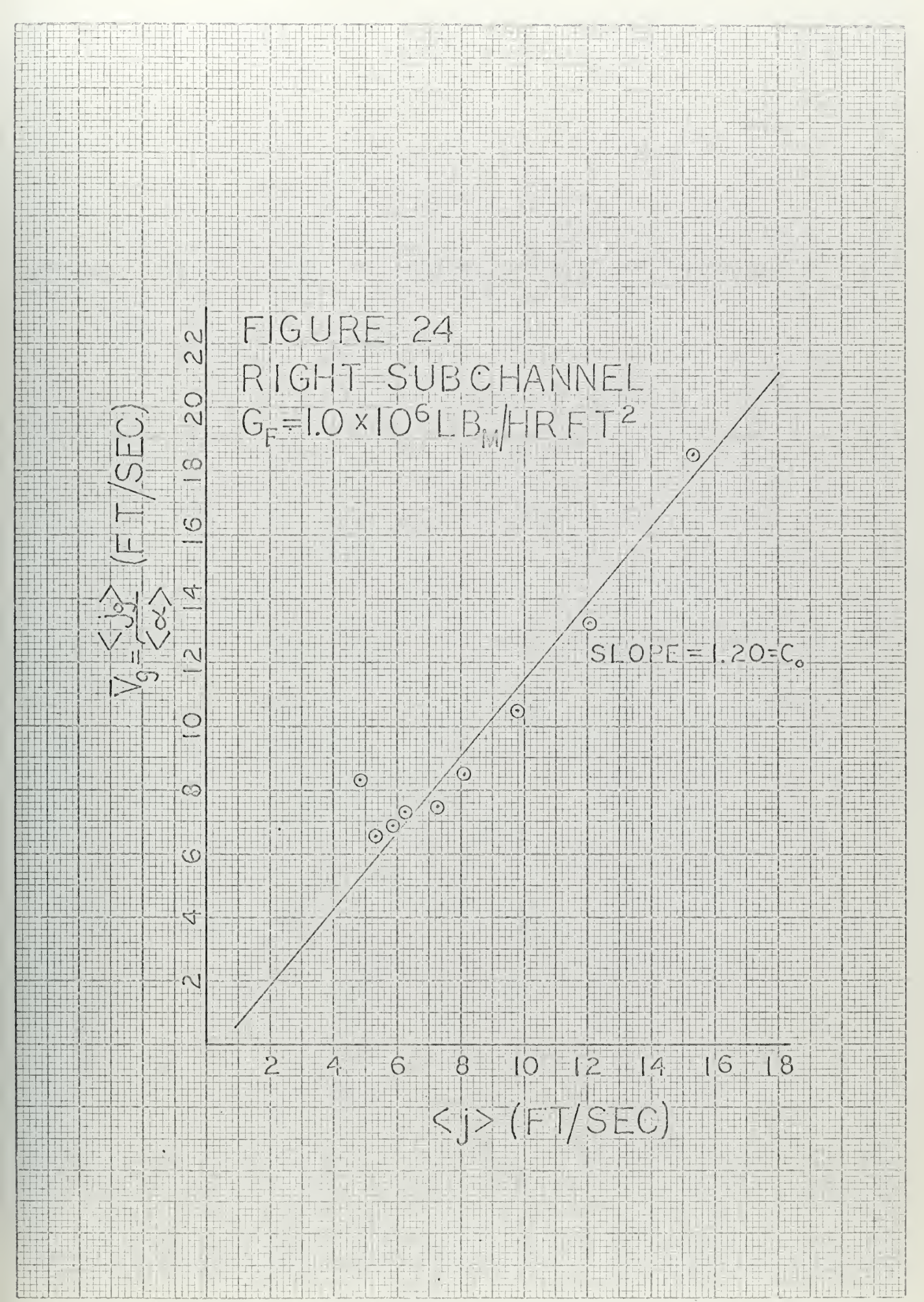
FIGURE 24
RIGHT SUBCHANNEL
$G_F = 1.0 \times 10^6 LB_M/HRFT^2$
$V_g = \frac{\langle j_g \rangle}{\langle \alpha \rangle}$ (FT/SEC)
2 4 6 8 10 12 14 16 18 20 22
SLOPE = 1.20 = C_o
2 4 6 8 10 12 14 16 18
$\langle j \rangle$ (FT/SEC)

FIGURE 25
RIGHT SUBCHANNEL
$G_F = 0.5 \times 10^6 LB_M/HR\,FT^2$

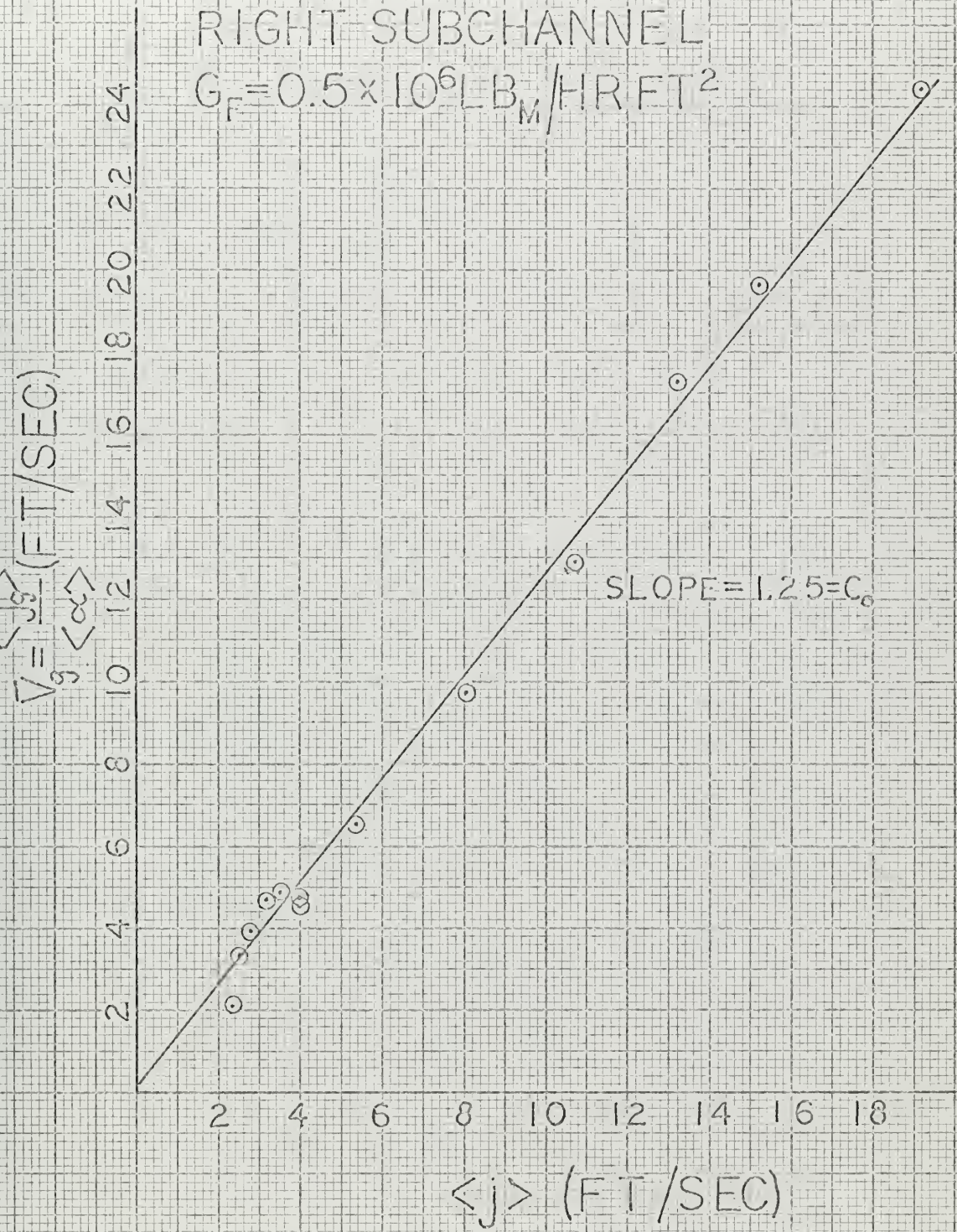

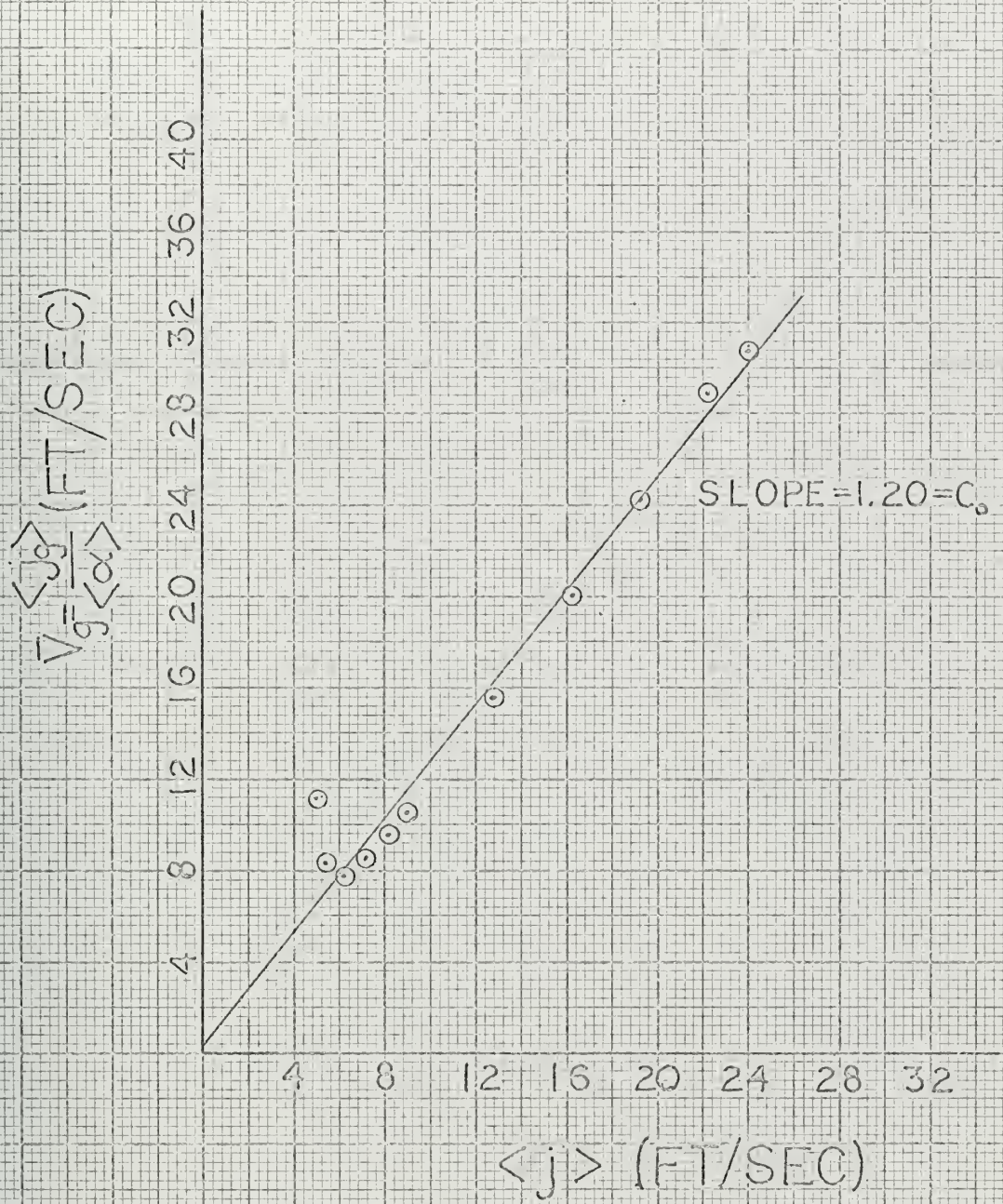

FIGURE 26
LEFT SUBCHANNEL
$G_F = 1.0 \times 10^6$ $LB_M/HR\ FT^2$

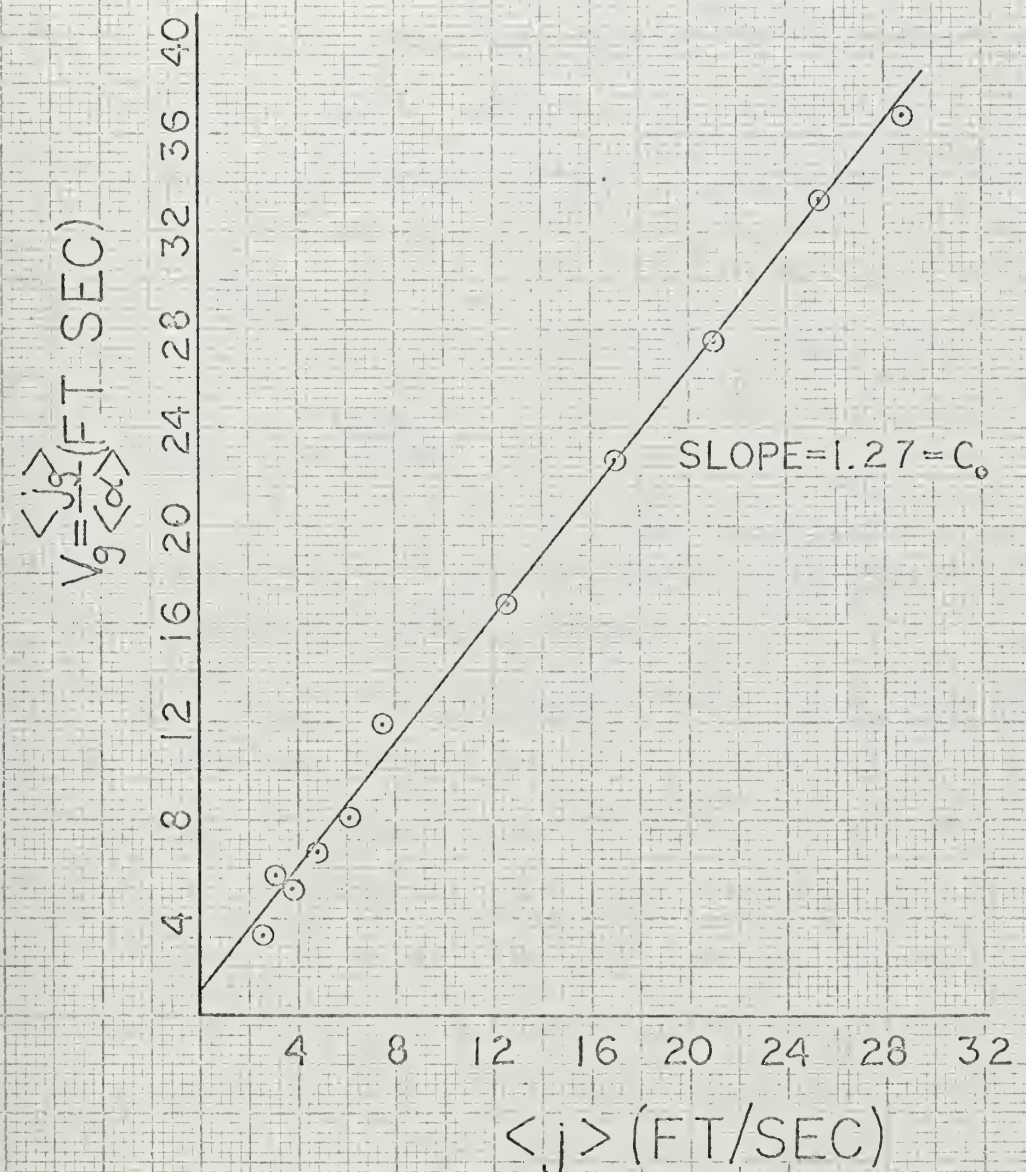

FIGURE 27
LEFT SUBCHANNEL
$G_F = 0.5 \times 10^6$ LB$_M$/HR FT^2

CHAPTER VI

Discussion of Results

The void fraction data obtained agree quite favorably with the various predictions plotted in Figures 12-15.

The Griffith slug flow correlation (12) was developed using round tubes, annuli, and circular shroud bundle geometries.

The void fraction under adiabatic conditions is given by:

$$R_g \equiv \alpha = \frac{Q_g}{Q_g + Q_f + V_b A}$$

where

$$V_b = K_1\sqrt{gD} + K_2\left(\frac{Q_f + Q_g}{A}\right)$$

D is defined differently for round tubes and other geometries, and K_1 and K_2 are also geometry dependent.

At first glance it would appear proper to utilize Griffith's rod bundle curves for estimation of the constants K_1 and K_2 in his correlation. Griffith's work entailed the use of a 2.0" shroud diameter bundle with seven rods. Keeping the shroud diameter constant, he varied the rod diameter, thereby altering the hydraulic diameter. The bubble velocities Griffith observed were bundle averages, not the average subchannel velocities of interest in the subchannels tested for this thesis. Hence the asymptotic values of K_1 and K_2 for round tubes were used in applying Griffith's correlation. When used in this manner, Griffith's correlation gave results which agreed very favorably with the data.

For the right subchannel, Griffith's correlation for round tubes produced void fractions somewhat less than those measured. In the left, more restricted subchannel, the Griffith prediction yielded a higher void fraction than that observed. Intuitively, one would anticipate generally lower void fractions here than in round tubes because of retardation of the liquid in sharp corners, etc. The fact that this same effect was not observed in the right subchannel is subject to speculation.

Comparison of Griffith's slug flow correlation with Zuber and Finley's (9) formulation gives the following relationships:

$$\alpha = \frac{Q_g}{Q_g+Q_f+AK_1\sqrt{gD}+K_2(\frac{Q_f+Q_g}{A})A}$$

$$= \frac{Q_g/A}{(1+K_2)(\frac{Q_f+Q_g}{A})+K_1\sqrt{gD}}$$

or in Zuber and Findlay's terminology

$$\langle\alpha\rangle = \frac{\langle j_g\rangle}{(1+K_2)\langle j\rangle+K_1\sqrt{gD}}$$

$$= \frac{\langle j_g\rangle}{C_o\langle j\rangle+\bar{V}_{gj}}$$

hence

$$C_o = 1+K_2 \text{ and } \bar{V}_{gj} = K_1\sqrt{gD}$$

The values of C_o obtained from the $\bar{V}_g$ versus $\langle j\rangle$ plots (Figures 24-27) yield values of K_2 of approximately 0.20 and 0.25. The

intercept on the ordinate axis, $\bar{V}_{gj}$, is difficult to specify exactly but seems to range from zero to about 0.5 FT/SEC.

Use of the asymptotic values for circular pipes for K_1 and K_2 and equivalent pipe diameter for D in Griffith's correlation agrees very closely with the information gleaned from the $\bar{V}_g$ versus <j> plots, corroborating the assumption that Griffith's correlation for cirular pipes applies to the geometry investigated.

Griffith's correlation used in this manner predicts values for C_o of 1.20 and $\bar{V}_{gj}$ of 0.34 and 0.39 FT/SEC for the left and right subchannels respectively.

The values of C_o of about 1.20 and 1.25 obtained for the two liquid superficial mass velocities of 1.0×10^6 and 0.5×10^6 $LB_m/HR\ FT^2$ respectively are in consonance with a flatter profile expected from doubling the water mass velocities. If Zuber and Findlay's definition of C_o for round tubes is used and the concentration and velocity profiles are assumed to be identical, exponent values of m and n of 3(G_f=0.5×10^6 $LB_m/HR\ FT^2$) and 4(G_f=1.0×10^6 $LB_m/HR\ FT^2$) are obtained for both subchannels.

The Lockhart-Martinelli void fraction predictions fall below the observed data in the region of intermediate void fractions. In the low and high void fraction regions the correlation seems to agree quite well with the data. This effect does not seem to be flow regime dependent at the lower end of the region of discrepancy, since it is present in the bubbly flow regimes for the right subchannel at

$G_f = 1.0 \times 10^6$ $LB_m/HR\ FT^2$ and in the slug flow regime for the other flow conditions analyzed. As the annular flow regime is approached, the Lockhart-Martinelli prediction agrees more closely with the data and may even give higher void fractions. Slug-annular flow was observed in the left subchannel at the higher gas flow rates investigated, but complete annular flow was never reached. The fact that the Lockhart-Martinelli predictions fall below the observed void fraction data, rather than above as one might expect, is unexplained.

The Cravarolo-Hassid correlation (13) for steam-water is included in the void fraction versus W_g curves for a comparison with their correlation and for steam-water and air-water mixtures.

The pressure gradient versus void fraction curves (Figures 16-19) agree quite favorably in shape with the curves predicted by the Lockhart-Martinelli correlation, but are consistently below the predicted values.

Scatter in pressure gradient data, particularly at higher void fractions in the slug flow regime can be attributed to two sources of error:

1) pressure drop fluctuations present in slug flow conditions, the effect of which could not be completely eliminated by the low pass filter, and
2) fluctuations in liquid mass flow rate caused by poor control by the water pressure regulator. These, though small, have a significantly higher effect on pressure gradient than on void fraction (such

fluctuations were more prevalent in the slug flow regime).

Average slip ratio, plotted versus gas mass flow rate, W_g, in Figures 20-23, seems to be in rough agreement with that predicted by the Marchaterre-Hoglund correlation. For the right subchannel, the observed slip ratios fell generally below the predicted values. On the other hand, observed slip ratios in the left subchannel were consistently greater than predicted values.

Since the slip ratio is related to void fraction,

$$S = \bar{V}_g/\bar{V}_f = \frac{X}{(1-X)} \quad \frac{(1-\alpha)}{\alpha} \frac{\rho_f}{\rho_g}$$

one would anticipate generally higher slip ratios for lower void fractions with equal quality flows in different geometries.

The observed slip ratio for the left, more restricted subchannel, then would probably be higher than that predicted for a more open (circular or rectangular) geometry, as is the case. The fact that the data for the right subchannel falls below the predicted curve, at least for all but the higher void fraction region, seems reasonable, since it may be even less restrictive than the average of Marchaterre and Hoglund's geometries.

Scatter in the slip ratio data may be attributed to the fact that the accumulation of errors in the void fraction measurement and flow measurement become magnified in this display of data. This is particularly true at lower void

fractions, where a small error in void fraction is multiplied beyond proportion in the slip ratio. The fact that the scatter is not uniform about a slip ratio of approximately unity at lower void fractions may be indicative of inadequate operation of the mixing device at a low gas mass flow rates.

An analysis of several representative electrical conductivity probe traces in the slug flow regime yielded bubble lengths varying from 1/2 - 6 inches with as much as 4 inches between bubbles. This data was obtained for the right subchannel at $G_f = 0.5 \times 10^6$ $LB_m/HR\ FT^2$ with $\alpha \cong .66$. In flow conditions such as these, a wide scatter in void fraction data occurred. The test section length, when compared with bubble lengths, was probably too small to achieve an accurate statistical average in a single sample.

A change in pressure at the level corresponding to the window location in the mixing test section will obviously affect void fraction. An experiment to determine the magnitude of this variation was conducted by approximately doubling the gage pressure at the window location for flow conditions in the bubbly flow regime. A decrease in void fraction of approximately .04 was observed.

It will be necessary to throttle the exit of either or both subchannels in the mixing experiments to produce equal pressure level on both sides of the window. It is expected that the effect on void fraction caused by such throttling can be predicted using the Lockhart-Martinelli correlation. It will be necessary, however, to substantiate this by experimental results.

CHAPTER VII

Conclusions

An experimental apparatus was designed, constructed and yielded satisfactory data for void fraction over a wide range of flow conditions. Higher void fraction regions beyond those covered ($\alpha_{max} \cong .70$) may be reached with modification or redesign of the air-water separators.

The data obtained agreed quite favorably with various correlations, although some discrepancy was present. Notably, the void fraction data were generally somewhat higher than the Lockhart-Martinelli predictions in the intermediate void fraction range. The Griffith slug flow correlation agreed quite well with the data in most cases.

Pressure gradient varied with void fraction in such a manner that it should be possible to match pressure level and pressure gradient under flow conditions of widely different void fractions in the mixing experiment.

Plots in the $\bar{V}_g$ versus <j> plane using Zuber and Findlay's formulation gave a rough indication of the peaking of the velocity and concentration profiles for varying superficial liquid mass velocities. Detailed profiles should be provided by other means, if needed.

The electrical conductivity probe was very useful in the identification of flow regimes and provided a means for estimating slug and bubble lengths. The design of the wall electrode for a normally non-conducting channel wall proved to be satisfactory.

Flow conditions in the subchannel geometries investigated are probably not representative of rod bundle average conditions, but rather representative of individual subchannels. Indeed, the purpose of these experiments was the simulation of subchannels. Preliminary indications suggest that the right subchannel, which models the flow region between four fuel rods, is representative of the actual geometry.

References

1) Rowe, D.S. and C.W. Angle, "Experimental Study of Mixing Between Rod Bundle Fuel Element Flow Channels During Boiling", Transactions ANS, 10, No. 2, (November, 1967), p. 655.

2) Todreas, N.E. and J.T. Rogers, "Coolant Mixing in Rod Bundles", Heat Transfer in Rod Bundles, ASME, 1968, New York.

3) Lahey, R.T., B.S. Shiralkar, and D.W. Radcliffe, Mass Flux and Enthalpy Distribution in a Rod Bundle For Single and Two-Phase Flow Conditions, (to be published).

4) Wallis, G.B., D.A. Steen, S.N. Brenner, and J.M. Turner, Joint U.S.-Euratom Research and Development Program, AT(30-1)-3114, Quarterly Progress Report, (January, 1964).

5) Lockhart, R.W. and R.C. Martinelli, "Proposed Correlation of Data for Isothermal Two-Phase, Two Component Flow in Pipes", Chemical Engineering Progress, 45, pp. 39-48, (1949).

6) Tong, L.S., Boiling Heat Transfer and Two-Phase Flow, New York, John Wiley and Sons, Inc., (November, 1966).

7) Rowe, D.S., Cross Flow Mixing Between Parallel Channels During Boiling, Part 1, BNWL 371, (March, 1967).

8) Rowe, D.S. and C.W. Angle, Cross Flow Mixing Between Parallel Flow Channels During Boiling, Part 3, BNWL 371, (January, 1969).

9) Zuber, N., and J. A. Findlay, "Average Volumetric Concentration in Two-Phase Flow System", ASME Annual Winter Meeting, New York (December, 1964).

10) Rohsenow, W.M. and H. Choi, Heat, Mass, and Momentum Transfer, Englewood Cliffs, New Jersey: Prentice-Hall, Inc., 1961.

11) Lahey, R.T. and R.A. Schraub, "Mixing, Flow Regimes and Void Fraction for Two-Phase Flow in Rod Bundles", Two-Phase Flow and Heat Transfer in Rod Bundles, Winter Annual ASME Heat Transfer Meeting, (November, 1969).

12) Griffith, P., "The Prediction of Low-Quality Boiling Voids", ASME Paper 63-HT-20.

13) Cravarolo, L. and A. Hassid, "Liquid Volume Fraction in Two-Phase Adiabatic Systems", Symposium on Two-Phase Flow, Ed. by P.M.C. Lacey, Devon, England: Department of Chemical Engineering, University of Exeter, (June, 1965), pp. 301-308.

14) Marchaterre, J.F. and B.M. Hoglund, "Correlation for Two-Phase Flow", Nucleonics, 20, No. 8, p. 142 (August, 1962).

15) Solomon, J.V., Construction of a Two-Phase Flow Regime Transition Detector, Master of Science Thesis, Massachusetts Institute of Technology, (June, 1962).

APPENDIX A

Two-Phase Conservation Equations and Void Fraction

A better understanding of the influence of void fraction on two-phase turbulent mixing may be achieved through examination of the relevant conservation equations.

Several multichannel computer programs have been developed using these equations to predict flow conditions and ultimately the burnout point for nuclear power reactors with ventilated parallel channels. The COBRA Code, (7), developed for single and two-phase flow, was selected as an example of present attempts to solve the problem of mixing as applied to burnout prediction.

The assumptions of the COBRA Code are as follows:

a) One-dimensional, two-phase flow is described by two average velocities, a gas velocity, $\bar{V}_g$, and a liquid velocity, $\bar{V}_f$. The velocity or slip ratio, $S=\bar{V}_g/\bar{V}_f$, is generally larger than one.

b) A static pressure drop can exist between adjacent subchannels, resulting in diversion cross flow

c) In diversion cross flow, the cross flow enthalpy is that of the subchannel from which it originates

d) Turbulent mixing can transfer enthalpy but not mass

Also implicit in the assumptions is the representation of subchannel variables, such as enthalpy, velocity, etc, by single average values.

Lahey and Schraub (11) suggested that a no net mass transfer approach cannot describe two-phase turbulent mixing adequately, and they propose an equal volume interchange as a more reasonable assumption from mixing length theory. This assumption requires experimental verification. The small amount of mixing data collected to date using the mixing apparatus indicate that for parallel channels subjected to equal pressure gradient there may be a net turbulent mixing flow by volume and by weight.

Another point raised by Lahey, Shiralkar and Radcliffe (3) is that the cross flow enthalpy is not always the same as that of the donor subchannel. One explanation for this condition may be a different velocity for each of the two phases in the diversion cross flow.

An example with two parallel and communicating subchannels has been selected to illustrate the use of the conservation equations, taking into consideration the effect of these proposed modifications to the equations presented in reference (7).

The following additional assumptions have been included in these equations:

a) A net turbulent mixing mass flow rate can exist in two-phase flow

b) The diversion cross flow liquid and vapor velocities may differ

c) An axial velocity, u, is defined in order to conserve the momentum of the mixture:

$$u = \bar{V}_f(1-X) + \bar{V}_g X = Gv'$$

where v' is defined such as to preserve the momentum of the mixture:

$$v' = \frac{(1-X)^2}{(1-\alpha)\rho_f} + \frac{X^2}{\alpha\rho_g}$$

The following mass continuity, energy and momentum equations apply to the control volume shown below for the momentum equation.

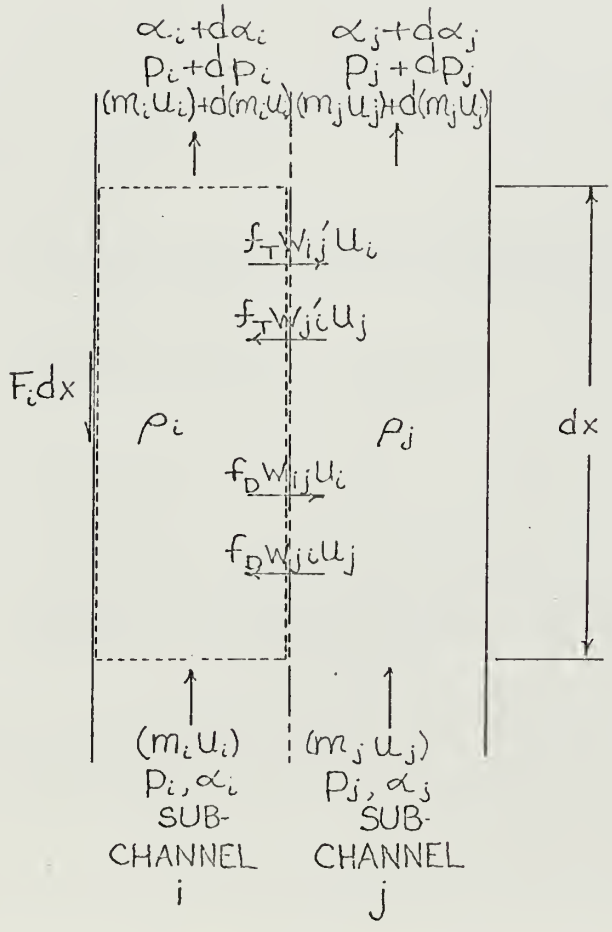

Control Volume Showing Momentum Fluxes

MASS CONTINUITY EQUATION

$$\frac{dm_i}{dx} = -w_{ij} + w_{ji} - w_{ij}' + w_{ji}'$$

where either w_{ij}, w_{ji}, or both are zero depending upon the existence and direction of diversion cross flow.

$$w_{ij}' = cG_{ij}' = c[(1-\alpha_i)\rho_f|\overline{u_{ij,f}}|+\alpha_i\rho_g|\overline{u_{ij,g}}|]$$

where $|u_{ij,f}|$ and $|u_{ij,g}|$ are appropriate measures of the turbulent components of the liquid and gas velocities perpendicular to the main axial flow (x direction), e.g., RMS values or averages of the absolute values. Changes of the void fraction, α_i, within the length dx are neglected in the above equation. Similarly,

$$w_{ji}' = cG_{ji}' = c[(1-\alpha_j)\rho_f|\overline{u_{ji,f}}|+\alpha_j\rho_g|\overline{u_{ji,g}}|$$

but $|\overline{u_{ij,f}}| = |\overline{u_{ji,f}}|$ and $|\overline{u_{ij,g}}| = |\overline{u_{ji,g}}|$

hence

$$\frac{w_{ji}'-w_{ij}'}{c} = G_{mixing} = (\alpha_i-\alpha_j)\rho_f|\overline{u_{ij,f}}|+(\alpha_j-\alpha_i)\rho_g|\overline{u_{ij,g}}|$$

The diversion cross flow terms, allowing for slip in the direction perpendicular to the main flow become

$$w_{ij} = c[(1-\alpha_i)\rho_f u_{ij,f} + \alpha_i\rho_g u_{ij,g}]$$

for flow from subchannel i to subchannel j and

$$w_{ji} = c[(1-\alpha_j)\rho_f u_{ji,f} + \alpha_j \rho_g u_{ji,g}]$$

for flow from subchannel j to i.

The appearance of the void fraction difference between adjacent subchannels in the turbulent mixing mass flow rates is a strong indication that void fraction can be used as a correlating parameter for mixing. If one considers the anticipated influence of void fraction on the fluctuating mixing velocities, $|\overline{u_{ij,g}}|$ and $|\overline{u_{ij,f}}|$, the assumption that void fraction is an important parameter in mixing seems even more conclusive.

Such a correlation need not necessarily be linear, since (as noted by Lahey and Schraub (11)) turbulent mixing seems to be strongly dependent on the two-phase flow regime, peaking somewhere in the slug flow regime. Judging from the disturbances caused by the passage of bubbles of various sizes, this suggestion seems reasonable.

ENERGY EQUATION

$$\frac{d(m_i h_i)}{dx} = q_i - w_{ij} h_i + w_{ji} h_j - w_{ij}' h_i' + w_{ji}' h_j'$$

Where, as before, either one or both of the diversion cross flow terms may be zero, depending on the existence and direction of the diversion cross flows.

Assuming a uniform void fraction distribution, the mixing energy transfer terms are

$$w_{ij}'h_i' = c[(1-\alpha_i)\rho_f h_f|\overline{u_{ij,f}}|+\alpha_i\rho_g h_g|\overline{u_{ij,g}}|]$$

$$w_{ji}'h_j' = c[(1-\alpha_j)\rho_f h_f|\overline{u_{ij,f}}|+\alpha_j\rho_g h_g|\overline{u_{ij,g}}|]$$

and the diversion cross flow energy transfer terms are

$$w_{ij}h_i = c[(1-\alpha_i)\rho_f h_f u_{ij,f} + \alpha_i\rho_g h_g u_{ij,g}]$$

$$w_{ji}h_j = c[(1-\alpha_j)\rho_f h_f u_{ji,f} + \alpha_j\rho_g h_g u_{ji,g}]$$

MOMENTUM EQUATION

$$g_c[A_i p_i - F_i dx - A_i(p_i+dp_i) - \frac{g\rho_i}{g_c} A_i dx]$$

$$= f_D w_{ij} u_i dx + f_T w_{ij}' u_i dx + m_i u_i + d(m_i u_i)$$

$$- (f_D w_{ji} u_j dx + f_T w_{ji}' u_j dx + m_i u_i)$$

Here, as in the COBRA Code, f_D and f_T account for non-uniform velocity and void fraction (concentration) profiles in a subchannel. The static average density is defined as

$$\rho_i = (1-\alpha_i)\rho_f + \alpha_i\rho_g$$

Expanding the axial momentum change term

$$d(m_i u_i) = m_i du_i + u_i dm_i = m_i d(G_i v_i') + u_i(w_{ji} - w_{ij} + w_{ji}' - w_{ij}')$$

$$= m_i[v_i' dG_i + G_i dv_i'] + u_i(w_{ji} - w_{ij} + w_{ji}' - w_{ij}')$$

$$= u_i dm_i + A_i G_i^2 dv_i' + u_i (w_{ji} - w_{ij} + w_{ji}' - w_{ij}')$$

$$= A_i G_i^2 dv_i' + 2u_i (w_{ji} - w_{ij} + w_{ji}' - w_{ij}')$$

$$\frac{F_i}{A_i} = \frac{f_i \phi_\ell^2 G_i^2}{2 g_c \rho_f D_{e,i}}$$

where f_i is the friction factor obtained assuming that all the flow is liquid and

$$\phi_\ell^2 = \frac{dp/dx)_{FR\ TP}}{dp/dx)_{FR\ \ell}}$$

is the two-phase frictional pressure drop multiplier.

Hence the momentum equation can be reduced to

$$-\frac{dp_i}{dx} = \underbrace{\frac{f_i \phi_\ell^2}{2 g_c \rho_f D_{e,i}} (G_i^2)}_{\text{friction pressure drop}} + \underbrace{\frac{G_i^2}{g_c} \frac{dv_i'}{dx}}_{\substack{\text{acceleration pressure} \\ \text{drop due to boiling}}}$$

$$+ \underbrace{\rho_i \frac{g}{g_c}}_{\substack{\text{gravity pressure} \\ \text{drop}}} + \underbrace{\frac{1}{g_c A_i} [u_i (w_{ij} (f_D - 2) + w_{ji} (2u_i - f_D u_j)}_{\text{momentum exchange terms}}$$

$$+ u_i w_{ij}' (f_T - 2) + w_{ji}' (2u_i - f_T u_j)]$$

It is apparent that a thorough study of the turbulent mixing phenomenon as it affects energy and momentum transfer must consider the concentration and velocity profiles. The lumped parameter approach may be justified, but the actual determination of a valid mixing length will be dependent upon

not only the mean void fraction and mean velocity in each channel but also on concentration and velocity distributions.

APPENDIX B

Description of the Electrical Conductivity Probes

The electrical conductivity probes were mounted near the discharge end of the entrance section for both left and right subchannels. In this location the probes allowed detection of flow regimes for each of the three test section configurations. Figure B-1 shows the flow probe installation.

The most difficult problem encountered in the construction of the probe was to provide a conducting electrode at the wall, since the wall material was lucite and non-conducting. Several methods were investigated, and a conducting silver epoxy paint was selected. This paste-like material (EPO-TEK 418H) was painted in a very thin coat on the lucite walls of the subchannels for a total subchannel length of six inches, centered at the flow probe. A portion of the conducting wall was formed by the brass strip separating the two subchannels. In the right subchannel an additional portion of the conducting wall was formed by the "plug" (brass flat bar) inserted in order to alter the hydraulic diameter of this subchannel. Outside connection with the wall electrode was accomplished by threading a small multistrand wire through a hole in the lucite wall and laying several strands in a shallow groove machined in the subchannel wall. The groove was then filled with the silver epoxy, covering the wire strands. This produced a sufficiently smooth surface. The epoxy was cured by careful use of a heat lamp, insuring that the temperature

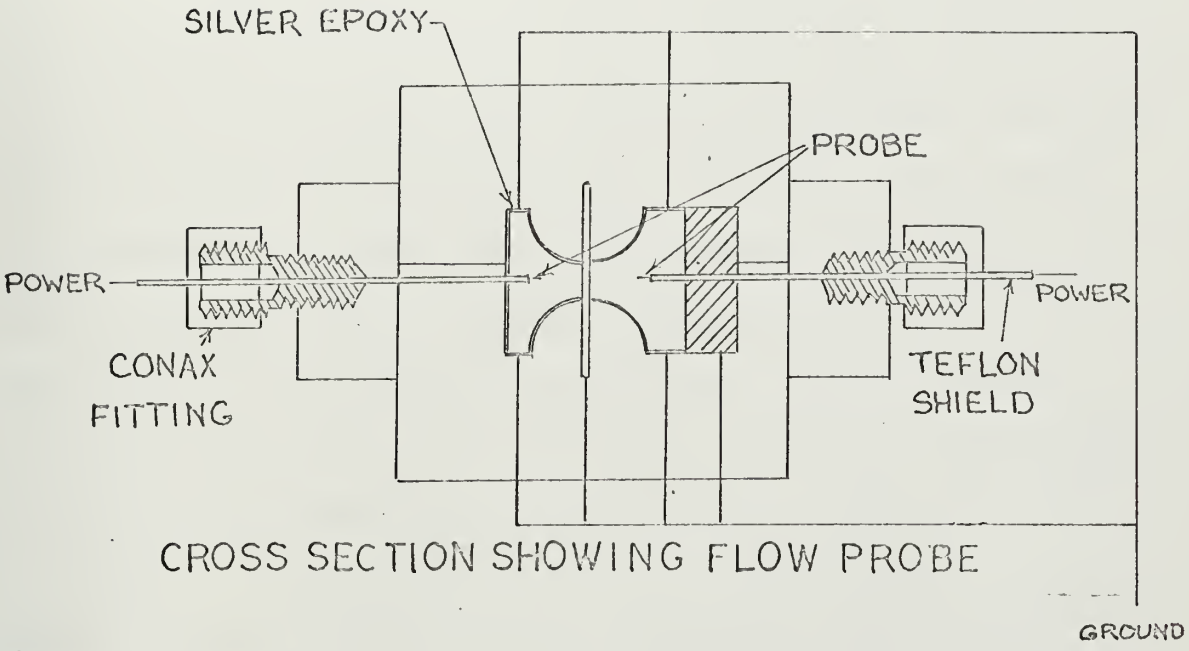

CROSS SECTION SHOWING FLOW PROBE

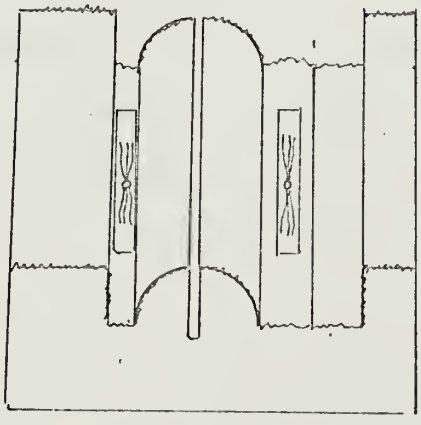

CUTAWAY VIEW SHOWING MULTI-STRAND WIRE RECESSED IN SUBCHANNEL WALLS

ELECTRICAL CONDUCTIVITY PROBE
FIGURE B-1

was not sufficiently high to cause plastic flow or warping of the lucite.

The probes themselves were cut from 24 gauge stainless steel spring wire, rounded at the probe tip and shielded with thin wall teflon spaghetti, except for an approximately 1/16" bare portion at the tip. The teflon shield was not wet by the liquid in the subchannel and consequently provided insulation between the probe tip and the wall electrode. The overall probe diameter, including the teflon shield, was about 0.035", approximately 8% and 10% of the hydraulic diameters of the right and left subchannels respectively. While a smaller probe would have been more desirable insofar as perturbation of the flow is concerned, it would not have had sufficient resistance to bending when buffeted by the flowing air-water mixture. A packing gland (Conax MIC-062A) was screwed into an external mounting block and provided a seal for the probe as it passed through the subchannel wall.

The electrical circuit was identical in principle to that described in reference (15). A six volt battery was used to supply power. Shielded cable was used for connections to eliminate noise.

Typical probe traces for various flow conditions are shown in Figure B-2. These Polaroid photographs of oscilloscope traces were taken for each of the data points recorded for the right subchannel.

In explanation of the photographs, signals near the top of the photographs indicate a current path through the water.

Signals at the bottom of the photographs indicate interruption of the current path by the passage of an air bubble.

Photographs of Typical Electric Flow Probe Traces

Figure B-2

APPENDIX C

Data

Right Subchannel $G_f = 1.0 \times 10^6$ $LB_m/HR\ FT^2$ $A = 1.855 \times 10^{-3}$ FT^2 $D_e = 3.85 \times 10^{-2}$ FT

W_g	P at window loc.	ρ_g at window loc.	Q_g at window loc.	Flow Regime	$\langle\alpha\rangle$	No.of samples	$\langle j_g\rangle$	$\bar{V}_g$	$\bar{V}_\ell$	S	$\langle j\rangle$	X	$\frac{dp}{d\ell}$
$\frac{LB_m}{HR}$	psia	$\frac{LB_m}{FT^3}$	$\frac{FT^3}{MIN}$				$\frac{FT}{SEC}$	$\frac{FT}{SEC}$	$\frac{FT}{SEC}$		$\frac{FT}{SEC}$	$\cdot 10^3$	$\frac{psi}{FT}$
10.45	30.18	0.1445	1.205	S	0.585	7	10.82	18.50	10.72	1.73	15.28	5.60	0.520
7.31	30.00	0.1437	0.848	B	0.575	3	7.62	13.25	10.50	1.26	12.08	3.93	0.529
5.11	29.94	0.1435	0.594	B	0.510	3	5.34	10.45	9.09	1.15	9.80	2.74	0.489
3.44	29.68	0.1415	0.406	B	0.434	3	3.65	8.42	7.87	1.07	8.11	1.91	0.456
2.60	28.86	0.1375	0.316	B	0.380	3	2.84	7.46	7.19	1.04	7.30	1.40	0.446
1.47	25.94	0.1235	0.198	B	0.243	3	1.78	7.32	5.89	1.24	6.24	0.793	0.427
1.09	25.05	0.1190	0.1522	B	0.200	3	1.369	6.84	5.57	1.23	5.83	0.588	0.430
0.664	23.74	0.1130	0.0979	B	0.134	3	0.879	6.55	5.15	1.27	5.34	0.358	0.427
0.273	22.55	0.1072	0.0424	B	0.046	3	0.381	8.28	4.68	1.77	4.84	0.147	0.430

B-S Transition at $W_g \cong 8.3$ LB_m/HR

Right Subchannel $G_f = 0.5 \times 10^6$ $LB_m/HR\ FT^2$

W_g	P at window loc.	ρ_g at window loc.	Q_g at window loc.	Flow Regime	$\langle\alpha\rangle$	No. of samples	$\langle j_g \rangle$	$\bar{V}_g$	$\bar{V}_\ell$	S	$\langle j \rangle$	X	$\frac{dp}{d\ell}$
$\frac{LB_m}{HR}$	psia	$\frac{LB_m}{FT^3}$	$\frac{FT^3}{MIN}$				$\frac{FT}{SEC}$	$\frac{FT}{SEC}$	$\frac{FT}{SEC}$		$\frac{FT}{SEC}$	$\cdot 10^3$	$\frac{psi}{FT}$
17.50	27.08	0.1330	1.896	S	0.697	7	17.02	24.40	7.38	3.31	19.25	18.5	0.390
10.55	25.06	0.1215	1.448	S	0.664	9	13.02	19.65	6.66	2.93	15.25	11.4	0.372
8.55	24.10	0.1170	1.220	S	0.635	7	10.95	17.25	6.12	2.82	13.18	9.21	0.353
6.33	23.02	0.1118	0.944	S	0.656	8	8.47	12.90	6.50	1.99	10.70	6.82	0.313
4.15	22.02	0.1070	0.646	S	0.594	3	5.80	9.77	5.50	1.77	8.03	4.48	0.313
2.08	20.42	0.0990	0.349	S	0.480	3	3.14	6.55	4.30	1.52	5.37	2.24	0.313
1.155	20.21	0.0980	0.196	B	0.388	3	1.76	4.53	3.66	1.24	3.99	1.25	0.308
1.112	19.49	0.0945	0.196	B	0.369	3	1.76	4.77	3.54	1.35	3.99	1.20	0.292
0.715	17.97	0.0855	0.139	B	0.2575	3	1.25	4.86	3.01	1.62	3.48	0.77	0.346
0.510	17.47	0.0838	0.101	B	0.194	3	0.906	4.67	2.78	1.74	3.14	0.55	0.350
0.311	17.62	0.0846	0.0616	B	0.1405	3	0.553	3.94	2.60	1.51	2.78	0.34	0.380
0.1555	16.93	0.0806	0.0321	B	0.086	3	0.288	3.35	2.52	1.33	2.52	0.17	0.389
0.0808	17.37	0.0826	0.0161	B	0.070	3	0.145	2.07	2.38	0.875	2.38	0.09	0.383

B-S Transition at $W_g \cong 1.62$ LB_m/HR

Left Subchannel $G_f = 1.0 \times 10^6$ $LB_m/HR\ FT^2$ $A = 1.267 \times 10^{-3}\ FT^2$ $D_e = 2.94 \times 10^{-2}$ FT

W_g	P at window loc.	ρ_g at window loc.	Q_g at window loc.	Flow Regime	$\langle\alpha\rangle$	No. of Samples	$\langle j_g \rangle$	$\bar{V}_g$	$\bar{V}_\ell$	S	$\langle j \rangle$	X	$\frac{dp}{d\ell}$
$\frac{LB_m}{HR}$	psia	$\frac{LB_m}{FT^3}$	$\frac{FT^3}{MIN}$				$\frac{FT}{SEC}$	$\frac{FT}{SEC}$	$\frac{FT}{SEC}$		$\frac{FT}{SEC}$	$\cdot 10^3$	$\frac{psi}{FT}$
12.05	28.28	0.1355	1.482	S-A	0.636	6	19.5	30.7	12.25	2.51	23.96	9.43	0.716
10.50	27.25	0.1303	1.342	S-A	0.614	6	17.7	28.8	11.55	2.50	22.16	8.22	0.696
8.44	26.08	0.1252	1.123	S	0.611	6	14.8	24.2	11.47	2.11	19.26	6.61	0.655
6.30	24.50	0.1182	0.888	S	0.586	6	11.7	20.0	10.80	1.85	16.16	4.95	0.600
4.17	22.84	0.1102	0.629	S	0.528	6	8.28	15.7	9.45	1.66	12.74	3.28	0.560
2.045	20.84	0.1005	0.339	B-S	0.430	6	4.46	10.4	7.83	1.33	8.92	1.61	0.563
1.617	20.04	0.0967	0.279	B	0.379	3	3.67	9.7	7.18	1.35	8.13	1.275	0.556
1.223	19.60	0.0945	0.216	B	0.339	3	2.84	8.38	6.75	1.34	7.30	0.965	0.530
.0766	18.96	0.0914	0.140	B	0.234	3	1.84	7.87	5.82	1.35	6.30	0.605	0.503
.0366	18.33	0.0885	0.069	B	0.110	3	0.908	8.25	5.02	1.64	5.37	0.289	0.487
.0213	17.82	0.0860	0.0413	B	0.048	3	0.544	11.3	4.69	2.42	5.00	0.169	0.413

Left Subchannel $G_f = 0.5 \times 10^6$ $LB_m/HR\ FT^2$

W_g	P at window loc.	ρ_g at window loc.	Q_g at window loc.	Flow Regime	$\langle\alpha\rangle$	No. of samples	$\langle j_g \rangle$	$\bar{V}_g$	$\bar{V}_\ell$	S	$\langle j \rangle$	X	$\frac{dp}{d\ell}$
$\frac{LB_m}{HR}$	psia	$\frac{LB_m}{FT^3}$	$\frac{FT^3}{MIN}$				$\frac{FT}{SEC}$	$\frac{FT}{SEC}$	$\frac{FT}{SEC}$		$\frac{FT}{SEC}$	$\cdot 10^3$	$\frac{psi}{FT}$
12.65	21.77	0.1050	2.01	S-A	0.719	4	26.5	36.8	7.95	4.62	28.73	19.6	0.510
10.45	20.72	0.0994	1.755	S-A	0.696	6	23.2	33.4	7.33	4.56	25.43	16.25	0.476
8.36	20.46	0.0982	1.420	S	0.676	6	18.7	27.6	6.88	4.00	20.93	13.03	0.443
6.25	19.50	0.0932	1.118	S	0.653	9	14.7	22.5	6.42	3.50	16.93	9.80	0.396
4.14	18.38	0.0880	0.785	S	0.619	10	10.35	16.7	5.85	2.86	12.59	6.50	0.353
2.025	17.74	0.0851	0.397	S	0.530	6	5.24	9.9	4.73	2.09	7.47	3.19	0.296
1.445	17.04	0.0818	0.295	S	0.480	6	3.89	8.1	4.28	1.89	6.12	2.28	0.291
0.925	16.68	0.0799	0.193	B-S	0.381	4	2.54	6.67	3.60	1.85	4.77	1.46	0.320
0.538	16.38	0.0785	0.1142	B	0.287	3	1.508	5.25	3.12	1.685	3.74	0.85	0.353
0.222	16.08	0.0771	0.0480	B	0.111	4	0.632	5.69	2.50	2.27	2.86	0.35	0.383
0.0811	15.92	0.0764	0.0177	B	0.069	6	0.233	3.38	2.39	1.42	2.46	0.128	0.350

Right Subchannel $G_f = 0.6 \times 10^6$ $LB_m/HR\ FT^2$

W_g	P at window loc.	ρ_g at window loc.	Flow Regime	$\langle\alpha\rangle$	No. of Samples	$\frac{dp}{d\ell}$	T_g inlet	T_f inlet
$\frac{LB_m}{HR}$	psia	$\frac{LB_m}{FT^3}$				$\frac{psi}{FT}$	°F	°F
15.6	29.92	0.1470	S	.673	7	.417	73.0	63.0
10.78	27.23	0.1310	S	.658	10	.420	80.0	59.5
8.45	26.20	0.1252	S	.631	13	.403	80.0	59.5
6.18	24.99	0.1195	S	.628	8	.394	80.0	59.5
4.11	23.15	0.1110	S	.559	6	.367	80.0	59.5
2.350	21.41	0.1010	B-S	.518	3	.406	80.0	59.5
2.03	21.64	0.1045	B	.500	3	.357	80.0	59.5
1.485	20.72	0.0990	B	.388	3	.350	80.0	59.5
1.320	20.42	0.0979	B	.366	3	.350	80.0	59.5
0.819	19.54	0.0917	B	.259	3	.360	80.0	59.5
0.394	18.88	0.0885	B	.138	3	.387	80.0	59.5
0.314	18.78	0.0880	B	.126	3	.387	80.0	59.5
0.0996	18.50	0.0865	B	.065	3	.400	80.0	59.5

Right Subchannel G = 0.7×10^6 $LB_m/HR\ FT^2$

W_g	P at window loc.	ρ_g at window loc.	Flow Regime	$\langle\alpha\rangle$	No. of Samples	$\frac{dp}{d\ell}$	T_g inlet	T_f inlet
$\frac{LB_m}{HR}$	psia	$\frac{LB_m}{FT^3}$				$\frac{psi}{FT}$	°F	°F
15.72	29.53	0.1430	S	0.651	6	.453	73.5	63.5
10.52	27.76	0.1345	S	0.611	6	.425	81.5	61
9.46	28.62	0.1375	S	0.612	6	.430	81.5	61
7.92	27.81	0.1345	S	0.616	13	.423	81.5	61
6.15	28.82	0.1390	S	0.586	7	.433	81.5	61
4.12	27.93	0.1340	B-S	0.524	9	.457	81.5	61
3.32	24.41	0.1170	B	0.522	5	.416	81.5	61
1.81	22.59	0.1082	B	0.434	3	.384	81.5	61
1.42	20.79	0.1045	B	0.342	3	.374	81.5	61
1.00	21.79	0.0995	B	0.272	3	.377	81.5	61
0.558	19.80	0.0950	B	0.160	3	.390	81.5	61
0.252	19.50	0.0935	B	0.057	3	.403	81.5	61

Right Subchannel $G = 0.8 \times 10^6$ $LB_m/HR\ FT^2$

W_g	P at window loc.	ρ_g at window loc.	Flow Regime	$\langle\alpha\rangle$	No. of Samples	$\frac{dp}{d\ell}$	T_g inlet	T_f inlet
$\frac{LB_m}{HR}$	psia	$\frac{LB_m}{FT^3}$				$\frac{psi}{FT}$	°F	°F
14.50	30.44	.1475	S	0.628	6	0.493	74.5	63.5
10.50	29.58	.1405	S	0.609	7	0.463	84.0	59.5
8.49	28.98	.1375	S	0.580	7	0.465	84.0	59.5
5.73	27.94	.1340	S	0.541	8	0.493	81.0	59.5
5.18	27.22	.1307	S	0.534	7	0.476	81.0	59.5
4.33	27.05	.1292	B-S	0.527	3	0.433	81.0	59.5
3.09	25.52	.1223	B	0.506	3	0.410	81.0	59.5
1.852	23.78	.1140	B	0.396	3	0.390	81.0	59.5
1.390	22.38	.1065	B	0.304	3	0.386	81.0	59.5
1.052	21.87	.1042	B	0.248	3	0.381	81.0	59.5
0.627	20.98	.1001	B	0.164	3	0.390	81.0	59.5
0.242	20.00	.0955	B	0.052	3	0.400	81.0	59.5

Right Subchannel $G = 0.9 \times 10^6$ $LB_m/HR\ FT^2$

W_g	P at window loc.	ρ_g at window loc.	Flow Regime	$\langle\alpha\rangle$	No. of Samples	$\frac{dp}{d\ell}$	T_g inlet	T_f inlet
$\frac{LB_m}{HR}$	psia	$\frac{LB_m}{FT^3}$				$\frac{psi}{FT}$	°F	°F
14.42	30.69	0.1486	S	0.606	7	0.527	74.5	63.5
10.55	29.93	0.1429	S	0.596	7	0.487	81	61
8.42	29.86	0.1427	S	0.554	10	0.503	81	61
6.22	29.82	0.1420	S	0.568	6	0.483	83	61
4.075	28.28	0.1375	B	0.504	3	0.450	83	61
2.690	26.93	0.1282	B	0.433	3	0.417	83	61
1.490	24.2	0.1150	B	0.290	3	0.403	83	61
1.470	24.9	0.1189	B	0.317	3	0.403	83	61
1.018	23.26	0.1105	B	0.209	3	0.369	83	61
0.622	22.46	0.1071	B	0.146	3	0.376	83	61
0.284	21.32	0.1015	B	0.056	3	0.413	83	61

B-S Transition at $W_g \cong 6.0$ LB_m/HR

Flow Regime Key

S-A Slug annular

S Slug

B-S Bubbly-Slug transition

B Bubbly

APPENDIX D

List of Equipment

Pressure Level Measurement

Stratham Pressure Transducer Model UC2

Stratham Model UR5 Universal Transducer Readout

Differential Pressure Measurement

Stratham 11639 PM 60 TC Pressure Differential Transducer

Ramapo Strain Gage Adapter Model S6A 100B

Hewlett Packard Model 412A DC Vacuum Tube Voltmeter

Air and Water Flow Measurement

Fisher-Porter Flowrators (various models)

Void Fraction Isolation Valves

Rockwood Figure 101 Ball Valves

(1 1/2" - main valves; 3/4" - bypass valve)

Electric Conductivity Probe

24 gauge stainless steel spring wire

MIC-062-A Conax Fittings

EPO-TEK 418H - High Temperature, Electrically Conductive Epoxy, (Epoxy Technology, Inc.)

Thesis
R277 Reese
118355
Void fraction in parallel channel boiling water reactors with application to two-phase turbulent mixing.